https://doi.org/10.5194/egusphere-2026-979
Preprint. Discussion started: 10 April 2026

Assessment of WRF-GHG model simulations during the CAFE-Brazil Campaign in Amazonia

Noelia R. Benavente[1,*], Santiago Botía[2], Luciana V. Rizzo[1], Angel Vara-Vela[1], Paulo Artaxo[1], Hella van Asperen[2], Felipe Santos da Silva[1], Flavio A. F. D'Oliveira[3,4], Horst Fischer[5], Michał Gałkowski[2,8], Theo Glauch[6], Alice Henkes[7], David Ho[2], Cléo Q. Dias-Júnior[4], Amauri C. P. Junior[1], Julia Marshall[7], Linda Ort[5], Ben-Hur M. Portella[1], and Luiz A. T. Machado[1,5]

[1]Physics Institute, University of Sao Paulo, Sao Paulo, Brazil
[2]Biogeochemical Signals Department, Max Planck Institute for Biogeochemistry, Jena, Germany.
[3]Department of Physics, Federal Institute of Pará (IFPA), Belém, PA, Brazil
[4]National Institute for Amazonian Research, Manaus, Brazil
[5]Max Planck Institute for Chemistry, Mainz, Germany
[6]Institut für Physik der Atmosphäre, Deutsches Zentrum für Luft- und Raumfahrt, Oberpfaffenhofen, Germany
[7]Leipzig Institute for Meteorology, Universität Leipzig, Stephanstraße 3, 04103 Leipzig, Germany
[8]Faculty of Physics and Applied Computer Science, AGH University of Kraków, Kraków, Poland

Correspondence: Noelia R. Benavente (rnoeliab@gmail.com)

Abstract. The Amazon Basin plays an important role in the global climate and carbon budget. Natural emissions and removals of CO_2 and CH_4 prevail in the wet season, dynamically responding to weather forcings. Accurate greenhouse gases (GHG) transport modeling is required to constrain the contribution of sources, sinks and atmospheric processes to observed mixing ratios. Kilometer-scale atmospheric models offer a compromise between computational cost and physical realism by partially resolving mesoscale processes that influence GHG transport in the Amazon. We evaluate the WRF-GHG model (Weather Research and Forecasting Model with GHG module) using CO_2 and CH_4 measurements from the Amazon Tall Tower Observatory (ATTO) and aircraft observations during the CAFE-Brazil campaign in January 2023. Simulations employed two domains centered at ATTO, MapBiomas land cover data, regionally adapted CO_2 biogenic flux parameters, and multiple wetland CH_4 emission configurations: an online process-based, a top-down optimized product, and process-based ensemble. The model correctly reproduced surface and vertical meteorological variables, particularly temperature and humidity. However, wind biases, and convective-driven boundary-layer dynamics affected tracer transport. Regionally adapted biogenic flux parameterizations improved representation of CO_2 temporal variability and net ecosystem exchange. For CH_4, CAMS Inversion-optimized flux product best reproduced observed concentrations and variability, while other inventories overestimated near-surface mole fractions. Aircraft comparisons highlighted the role of wetland emissions and wind-driven transport in regional CH_4 enhancements. These findings underscore the importance of improving the biogenic flux parameterizations and kilometer-scale resolution to enhance GHG modeling in complex tropical environments.

https://doi.org/10.5194/egusphere-2026-979
Preprint. Discussion started: 10 April 2026

1 Introduction

The Amazon Basin plays a relevant role in the global carbon cycle, storing carbon in its soils and biomass and accounting for 14% of the gross primary productivity of terrestrial ecosystems (Zhao and Running, 2010). It is also a natural source of methane (CH_4) from wetlands, representing 8% of global emissions (Basso et al., 2021; Beck et al., 2012). Regional atmospheric transport models are a useful tool for investigating the relative importance of processes driving greenhouse gas (GHG) emissions, removals and transport, connecting local surface fluxes to mesoscale. In atmospheric inversion systems, regional models are typically nested under global atmospheric models (Rödenbeck et al., 2009), refining the representation of surface and atmospheric processes in the area of interest (e.g., Botía et al., 2025a). Accurate quantification of carbon dioxide (CO_2) and CH_4 fluxes and their spatial distributions relies on robust observational data and bottom-up emission estimates, complemented by high-resolution atmospheric transport simulations that better represent key processes governing greenhouse gas distributions (Colas et al., 2020). Coarse-resolution global models often misrepresent convection, boundary-layer processes, and sub-grid heterogeneity, particularly in tropical regions such as the Amazon, where atmospheric and surface processes are highly complex (Beck et al., 2012; Molina et al., 2015).

Some research also highlights the critical role of high-resolution atmospheric modeling and aircraft measurements in improving GHG modeling capabilities. For instance, high-resolution CO_2 simulations using the Weather Research and Forecasting model with greenhouse gas modules (WRF-GHG) at 1x1 km resolution over the Kanto region of Japan have demonstrated improved representation of aircraft observations between 0–3 km altitude, compared to coarser 27x27 km simulations (Bisht et al., 2023, 2025). While high-resolution simulations can improve the representation of vertical distribution of GHGs, it is important to recognize that they do not fully resolve all challenges in GHG quantification, particularly in the lower atmosphere (Gerbig et al., 2008). Accurate simulation of GHG transport is important to reduce uncertainties in flux estimates by atmospheric inversions. Wilson et al. (2016) reported biases in the simulated background mixing ratios of CH_4 in Amazonia due to inaccurate representation of the interhemispheric transport of air masses. Improper representation of the near surface vertical mixing can also lead to biases in flux estimates, when adjusting the simulated GHG vertical profiles to observations in the boundary layer (Gerbig et al., 2008). This is especially true for CH_4, as it is short-lived and typically shows stronger vertical gradients compared to CO_2 (Basso et al., 2021). Beck et al. (2013) reported significant mismatches between CH_4 simulated vertical profiles and observations under convective weather conditions, during the BARCA (Balanço Atmosférico Regional de Carbono na Amazônia) aircraft campaign in Amazonia. In addition to atmospheric transport, proper representation of GHG emission and removal processes are important to accurately simulate the spatial and temporal distribution of GHGs in atmospheric transport models. Beck et al. (2012, 2013) reported significant variations in the modeled CH_4 mixing ratios in Amazonia, depending on the choice of wetland emission model and inundation map in the WRF-GHG model. Wetland adjustment factors between -76% and +9% were reported to match CH_4 simulations and observations during the BARCA aircraft campaign. While these simulations provided valuable insights into CH_4 dynamics in the Amazon, they also emphasize the need for more accurate wetland inundation data, and better convective and boundary layer parametrizations to enhance model

https://doi.org/10.5194/egusphere-2026-979
Preprint. Discussion started: 10 April 2026

performance.

In this study, we evaluate WRF-GHG simulations using CO_2 and CH_4 measurement over the Brazilian Amazon during January 2023, coinciding with the CAFE-Brazil campaign. During this campaign, atmospheric measurements were conducted using the German High Altitude and Long Range Research Aircraft (HALO) under predominantly pristine atmospheric conditions (Curtius et al., 2024; Nussbaumer et al., 2024). The model setup builds upon previous WRF-GHG applications in the region but introduces several key advances in comparison to previous studies (Beck et al., 2012, 2013). Land surface representation is improved through the replacement of the default WRF land-use dataset with MapBiomas land cover data (Souza et al., 2020). Biogenic CO_2 fluxes were estimated using the online Vegetation Photosynthesis and Respiration Model (VPRM), incorporating a region-specific VPRM parameters set (Botía et al., 2025a) to improve the simulation of carbon fluxes across Amazonian forests and the adjusted Joint UK land environment simulator (JULES) model as described by Prudente Junior et al. (2025). For CH_4, this study goes beyond previous applications by explicitly comparing multiple wetland emission representations, including online process-based wetland emission model, a top-down optimized wetland flux field, and process-based flux fields ensemble. This approach allows us to assess the contribution of wetlands to regional CH_4 variability and evaluate the sensitivity of model results to different emission inventories.

The objectives of this study are to (1) assess the model's ability to reproduce surface-based observations from the ATTO site as well as vertical profiles and spatial variability measured by the HALO aircraft, and (2) identify and characterize simulation limitations that affect the transport, mixing, and dilution of GHGs, thereby improving the interpretation of simulations. A secondary objective is to evaluate and refine the WRF-GHG model configuration for application in regional modelling over tropical regions, including e.g. downscaling of future climate scenarios, which will be addressed in subsequent work. By adjusting physical parameterizations to better represent the Amazon region, this study proposes a recommended model setup for simulating future conditions and explicitly documents its limitations. This framework provides a robust foundation for modeling net ecosystem exchange under future scenarios and supports further investigations within the context of Shared Socioeconomic Pathways (SSPs).

2 Data and Observation Platforms

2.1 Ground based observations

Ground-based observational data at the INSTANT tower (2°08.64′S, 58°59.99′W) were used for the period 1–31 January 2023. This tower is located approximately 650 meters away from the Amazon Tall Tower Observatory (ATTO; https://www.attodata.org/), situated within the Uatumã Sustainable Development Reserve in central Amazonia, northern Brazil (Fig. 1). The INSTANT tower has a height of 81 meters and provides vertical profiles of meteorological variables, greenhouse gas (GHG) mole fraction, and H_2O and CO_2 flux (van Asperen et al., 2024; Botía et al., 2025b) in the central Amazon. It is equipped with fast-response 3D sonic anemometers, infrared gas analyzers (IRGA), and thermohygrometers at multiple heights (Mendonça et al.,

https://doi.org/10.5194/egusphere-2026-979
Preprint. Discussion started: 10 April 2026

2025). These measurements were used to estimate surface–atmosphere exchange processes for CO_2 via the eddy covariance method. Continuous measurements of CO_2 and CH_4 at five heights along the tower were made using a Picarro G2401 (van Asperen et al., 2024), with data from 81 meters selected for this study to examine GHG dynamics above the canopy. Meteorological variables—including wind speed and direction, temperature, humidity shortwave radiation and planetary boundary layer (PBL)—were also selected at the same height (81 meters) and included in the analysis to complement the GHG data. The PBL was estimated by a CHM15k ceilometer installed at the ATTO experimental site (Sousa et al., 2023). Due to the dense forest environment surrounding the ATTO site, a complementary site named Campina-ATTO was established approximately 4 km away, in a more open forest area, to accommodate ground-based remote sensing instrumentation (Cecchini et al., 2025). At Campina-ATTO, radiosonde data were collected from January 11 to 26, 2023, with an average of 10 radiosondes launched at different times of the day. These instruments were used to evaluate the performance of the WRF model, focusing on both near-surface meteorological conditions and vertical atmospheric profiles.

In addition to the INSTANT, and Campina-ATTO observations, surface meteorological data from the Brazilian National Institute of Meteorology (INMET) were employed to assess the sensitivity of the model to different physical parameterizations and surface representations. Given the large number of INMET stations (colored circles inside Figure 1) and the exploratory nature of this sensitivity analysis, a comprehensive description of the station network, data processing, and evaluation methodology is provided in the Supplementary Material (section A). Accordingly, Table 1 summarizes only the core observational datasets used for the main model evaluation, while the INMET-based analyses are documented separately.

2.2 CAFE-Brazil Aircraft Campaign

CAFE-Brazil (Chemistry of the Atmosphere: Field Experiment in Brazil; Curtius et al., 2024; Nussbaumer et al., 2024) was a major atmospheric chemical campaign focused on studying the interactions between clouds and aerosols, and in the new particle formation in the upper troposphere. The campaign took place from end of November 2022 until end of January 2023, only measuring in Brazil in December 2022 until January 2023. As part of the campaign, the German High Altitude and Long Range Research Aircraft (HALO) research aircraft performed 22 flights in total between November 30, 2022 and January 29, 2023. The aircraft flew at altitudes ranging from 0.3 to 13.8 km across the Amazon region, spanning latitudes from 11°33′S to 4°40′N and longitudes from 72°33′W to 33°50′W. These flights aimed to collect data on aerosols and gases at various altitudes. Equipped with advanced instruments, the aircraft provided real-time atmospheric data, including measurements of aerosols, traces gases, and basic atmospheric parameters. The Research Flight 15 (RF15) mission (Table 1), which took place on January 14, 2023, was chosen to validate the WRF-GHG model, focusing on meteorological data and CH_4 mixing ratios. The latter was measured via quantum cascade laser infrared absorption spectroscopy (QLAS) from Airborne Tropospheric Tracer In-situ Laser Absorption spectrometer (ATTILA; Ort et al., 2024). Dry corrected CH_4 (using N_2O data, see Ort et al., 2024), was averaged from 1Hz data to 300s averages to increase data precision (15.9 %, Accouracy: 5.5 % on 1 Hz in-flight calibration gas mixing ratios of 1990 ppbv) (Ort et al., 2024). The mission lasted 9 hours, from 11:58 to 20:48 UTC (see Fig. 1b). This study focuses on the wet season, a period when fire-related emissions are minimal.

https://doi.org/10.5194/egusphere-2026-979
Preprint. Discussion started: 10 April 2026

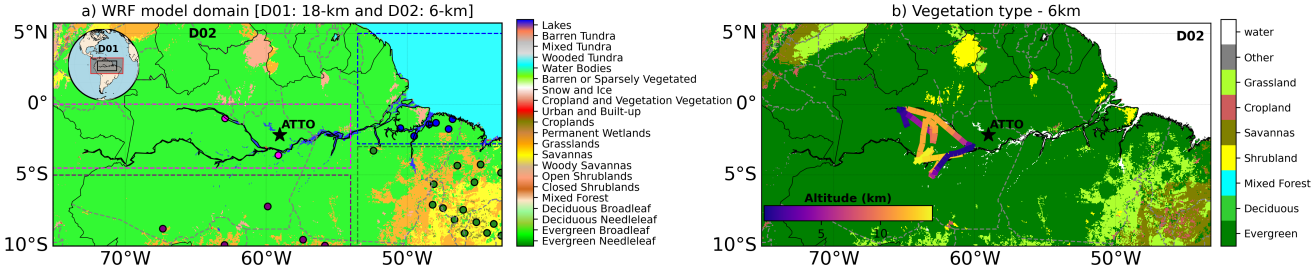

Figure 1. (Left panel) The study area and the WRF model domains (D01 and D02) are shown, with the color bar representing the MapBiomas land cover classification. The star shows the ATTO site location, while the circles represent INMET meteorological stations. Dashed squares delimit four different regions used for validation of simulated meteorological variables (refer to the supplementary material). (Right panel) The map illustrates the vegetation types over the nested domain used in the VPRM module, as well as the aircraft trajectory for the CAFE-Brazil RF15 mission. The color bar shows the altitude along the trajectory.

Table 1. Observation sites used to validate the WRF-GHG model

Sites	Location	Height	Variables
INMET network*	"within D02 - Fig. 1"	surface	T_{2m}, RH_{2m}, WS_{10m} and WD_{10m}
ATTO-Campina	2.181°S; 59.02°W	< 15 km	T_θ, SH and WS
INSTANT tower	2.144°S; 58.99°W	at 81 m	T_{81m}, WS_{81m}, WD_{81m}, PBL, SW_{in} and Prec, CO_2 and CH_4
Flight-CAFE Brazil	3.03°S; 60.04°W	< 15 km	T_θ, SH, WS, V_z and CH_4

T_θ: Potential temperature; SH: specific humidity; V_z: vertical velocity

* The list of INMET stations can be found in the supplementary material, Table S1.

3 Model Description and Experimental Setup

3.1 WRF-GHG Model Configuration

In this study we integrate in-situ observations with high-resolution model simulations to assess the performance of the Weather Research and Forecasting model coupled with the Greenhouse Gases module (WRF-GHG; Beck et al., 2011). WRF-GHG is built upon the Advanced Research WRF model (version 4.2.1) and incorporates the Vegetation Photosynthesis and Respiration Model (VPRM; Ahmadov et al., 2007) and the Kaplan-Ridgwell wetland model (Ridgwell et al., 1999; Kaplan , 2002) to simulate biosphere-atmosphere carbon and methane fluxes. By coupling meteorological dynamics with biogenic, anthropogenic, and biomass burning emissions, WRF-GHG simulates the atmospheric transport of GHG, treated as inert species. We apply the model at a 6-km horizontal resolution in its nested domain to simulate CO_2 and CH_4 mole fractions near the Amazon Tall Tower Observatory (ATTO) site. The model uses a Lambert Conformal Conic (LCC) projection for spatial mapping. Two domains with different grid resolutions: the coarse domain (D01) contains 348x161 grid points at 18-km resolution, and the nested domain (D02) contains 592x295 grid points at 6-km resolution (as shown in Fig. 1 and Table 2). The outermost domain

https://doi.org/10.5194/egusphere-2026-979
Preprint. Discussion started: 10 April 2026

(D01) encompasses a large region of South America, including the Pacific and Atlantic Oceans and the northern Amazon basin, covering ∼ 6,228 x 2,880 km^2. This wide coverage allows for the realistic simulation of synoptic-scale influences on regional GHG dynamics. Both domains have 51 vertical levels, with a constant 50 m interval within the first 2 km of altitude, gradually increasing to the model's top at 100 hPa (∼ 16.5 km). Simulations were conducted for the period from 00:00 UTC on January 1st to 00:00 UTC on January 31st, 2023, covering the time frame of the CAFE-Brazil RF15 and the ATTO measurements. A 10-day spin-up period was used from January 1-10 to allow the model to remove any residual influence of the intital conditions before the analysis period. The physical parameterizations applied in this study (see Table 2) were selected based on sensitivity analyses designed to identify the most suitable configuration. The sensitivity analyses are described in the supplement section A.

To streamline the data pre-processing and model setup, we developed WRF-GHG-Prepy, a Python-based pre-processor available on GitHub: https://github.com/rnoeliab/WRF-GHG-Prepy. This tool automates the integration of emission inventories, land cover maps, and VPRM inputs into the WRF-GHG workflow. A complete description of this pre-processing system is provided in Appendix A. The model simulations were performed using re-initialization cycles, a strategy adopted to reduce long-term drift and maintain meteorological consistency (Ho et al., 2024). A detailed description of the workflow used to run WRF-GHG, including the re-initialization procedure, is presented in the supplement section C. For the incoming mole fractions from outside the continent, a background tracer is used to monitor the evolution of GHG concentrations across the domain within the WRF-GHG framework. Additionally, source-specific tracers are used to track emissions from different sectors-namely anthropogenic, biomass burning, and natural biogenic sources. This enables a detailed breakdown of the total simulated concentrations.

3.2 Initial and Boundary Conditions

Meteorological initial and lateral boundary conditions were derived from the ERA5 reanalysis (Hersbach et al., 2020), produced by the European Centre for Medium-Range Weather Forecasts (ECMWF). ERA5 offers global coverage at 0.25 ° spatial resolution, with 137 vertical levels and an hourly temporal resolution; however, for this study, a 6-hour temporal resolution was considered. GHG concentrations for CO_2 and CH_4 were initialized using the Copernicus Atmospheric Monitoring Service (CAMS) global Inversion-optimized concentrations, hereafter referred to as CAMS-Inversion-CO_2 (version: FT24r1; CAMS, 2023a) and CAMS-Inversion-CH_4 (version: v23r1; CAMS, 2023b) , respectively. Although both systems follow a similar Bayesian inversion framework that assimilates satellite and in-situ observations to generate three-dimensional atmospheric concentration fields, they differ in their treatment of fluxes, chemical processes and also transport model. CAMS-Inversion-CO_2 provides data at a horizontal resolution of 0.7° (∼ 78 km) in latitude and 1.4° (∼ 155 km) in longitude, with 79 vertical levels. In contrast, CAMS-Inversion-CH_4 provides data at a horizontal resolution of 1° x 1° (∼ 110 km around equator), with 34 vertical levels. Updated every six hours, the CAMS-Inversion provides boundary and initial conditions that are consistent with atmospheric measurements of CO_2 and CH_4.

https://doi.org/10.5194/egusphere-2026-979
Preprint. Discussion started: 10 April 2026

Table 2. Configurations used in WRF-GHG model with two-way nesting system

Model configuration	WRFV3 description	
Vertical coordinate	51 levels (top pressure-10hPa)	
Updated surface maps	Vegetation Map: MapBiomas 2015 - Collection 3.1 (over D01 and D02) Greenness Fraction: MODIS NDVI 30s 1992–1993 Albedo: MODIS NDVI 30s 1992–1993; Soil moisture: GPNR 0.25° daily	
Simulation period	01-31 January 2023 - 10 days for spin-up	
Horizontal resolution	D01: 18x18 km (348 x 161) and D02: 6x6 km (592 x 295)	
Meteorological initial/boundary condition	ERA5 reanalysis data (Hersbach et al., 2020)	
Chemical Initial/boundary condition	CAMS global Inversion-optimized concentrations (CO_2: FT24r1; CH_4: v23r1; CAMS, 2020)	
Anthropogenic emissions	EDGAR v6.0 - GHG (Ferrario et al., 2021)	
Biogenic emissions	VPRM code (Mahadevan et al., 2008)	
Fire emissions	GFAS version 1.2 (Kaiser et al., 2012)	
Domains	D01	D02
Microphysics scheme	WRF Single-moment 6-class Scheme	WRF Single-moment 6-class Scheme
Cumulus parameterization	Grell-Devenyi Ensemble Scheme	turn-off
Planetary boundary scheme	Yonsei University Scheme	Yonsei University Scheme
Short-wave and Long-wave radiation scheme	RRTMG Schemes	RRTMG Schemes
Land surface model	Unified Noah Land Surface	Unified Noah Land Surface
Surface Layer	Revised MM5	Revised MM5

3.3 Emission Inventories and Surface Fluxes

3.3.1 Anthropogenic and Biomass Burning Emissions

Anthropogenic fluxes were derived from the Emission Database for Global Atmospheric Research version 6.0 (EDGAR v.6.0; Ferrario et al. (2021)). This dataset provides annual global emissions of CO_2 and CH_4 at 0.1° spatial resolution, including contributions from energy production, industry, transportation, and waste (Janssens-Maenhout et al., 2019). EDGAR inventories are based on bottom-up methods aligned with IPCC guidelines and complement national reporting under the Paris Agreement. For this study, daily emission factors were applied to represent diurnal variations in CO_2 and CH_4 emissions. Emissions from EDGAR were assumed to be emitted at the surface, which is generally sufficient for CH_4. While this approximation may not be ideal for CO_2, it is reasonable in the context of the Amazon region, where industrial and power plant activities are minimal, particularly around the ATTO site. Biomass burning emissions were sourced from the Global Fire Assimilation System (GFAS v1.2), which assimilates satellite fire radiative power (FRP) data, including from MODIS sensors, to produce

https://doi.org/10.5194/egusphere-2026-979
Preprint. Discussion started: 10 April 2026

daily GHG emission estimates at 0.1° spatial resolution (Kaiser et al., 2012). However, little emphasis was placed on biomass burning emissions in this study, as during this time of the year, such emissions are generally negligible in the Amazon region because the wet season corresponds to low fire occurrence in the seasonal pattern.

3.3.2 Biogenic CO_2 Fluxes - Vegetation Photosynthesis and Respiration (VPRM)

The WRF-GHG framework calculates biogenic CO_2 fluxes online using the Vegetation Photosynthesis and Respiration Model (VPRM) developed by Mahadevan et al. (2008) and implemented into a coupled WRF framework by Ahmadov et al. (2007), which employs empirical formulations and remotely sensed parameters to simulate biosphere-atmosphere carbon exchange. Net ecosystem exchange (NEE) is computed as the difference between gross primary production (GPP) and ecosystem respiration. GPP is estimated using a light-use efficiency approach that incorporates meteorological drivers, such as air temperature (T) and photosynthetically active radiation (PAR), along with satellite-derived indices like the Enhanced Vegetation Index (EVI) and the Land Surface Water Index (LSWI). These indices are computed from MODIS surface reflectance bands (MOD09A1 product; Reflectance 8-Day L3 Global 500m), interpolated to daily intervals, and smoothed using a lowess filter (Glauch et al., 2025).

VPRM parameters require calibration for regional applications (Mahadevan et al., 2008), with key parameters including maximum light-use efficiency (λ_0), photosynthetically active radiation at half-saturation (PAR_0), and respiration parameters (α and β). The full set of VPRM parameters also includes T_{min}, T_{max}, T_{opt}, and T_{low}, which are drawn from the literature to avoid numerical instabilities. The values for λ_0, PAR_0, α and β are typically derived by calibrating VPRM-simulated NEE against eddy-covariance flux tower measurements. In this study, the calibrated values for λ_0, PAR_0, α and β were obtained from the previous work by Botía et al. (2025a). These are presented in Table S4 of the supplementary material. Specific parameter values are assigned to each vegetation class to capture distinct physiological behaviors. Land-cover data were obtained from the MapBiomas dataset and subsequently reclassified to match the vegetation classes used by the VPRM module. For example, the VPRM “evergreen” class combines MapBiomas classes such as "forest formation" and "floodable forest", while other VPRM classes were formed by grouping relevant MapBiomas categories accordingly (Figure 1b and Table S5). This ensures ecosystem-specific characteristics are accurately represented in the simulations.

3.3.3 Biogenic CH_4 Fluxes - Wetland Emission Inventories

For the simulation of CH_4 mole fractions, three different wetland emission configurations were used to represent the range of uncertainties in wetland CH_4 fluxes. The Kaplan model (Kaplan , 2002), implemented online within WRF-GHG, estimates biogenic CH_4 fluxes based on wetland parameterizations (Beck et al., 2011). Biogenic CH_4 fluxes are estimated based on static inundation and soil carbon pool maps, and on the dynamical variables: soil temperature and humidity (Beck et al., 2013). In the Kaplan model, the wetland extent is provided by the Bergamaschi et al. (2007) inundation map, while the soil carbon pool was estimated by the Lund–Potsdam–Jena (LPJ) dynamic vegetation model (Beck et al., 2012). Additionally, the model includes CH_4 emissions from termites following Sanderson (1996) and soil CH_4 fluxes calculated using the process-based

https://doi.org/10.5194/egusphere-2026-979
Preprint. Discussion started: 10 April 2026

scheme of Ridgwell et al. (1999), both computed internally within WRF-GHG using static parameters and WRF meteorological fields. In addition to Kaplan model, two CH_4 emission inventories were used in WRF-GHG, linked to separate tracers, allowing the comparison of results. The first inventory is the CAMS global Inversion-optimized flux product (v22r2), which estimates wetland CH_4 emissions through an atmospheric inverse modeling framework. This system assimilates atmospheric CH_4 observations from satellites and in-situ measurements and combines them with a transport model to infer fluxes, providing an observationally constrained alternative to process-based inventories. The spatial resolution is 1° x 1°, with a monthly-mean output frequency. The second inventory corresponds to the WetCHARTs (v131) six-model ensemble (Bloom et al., 2021), which includes the variants: Wetch-2913, Wetch-2923, Wetch-2933, Wetch-2914, Wetch-2924 and Wetch-2934. As described in Table 3 of the WetCHARTs documentation (Bloom et al., 2021), each ensemble member is identified by a four-digit code, with each digit specifying one of four model configurations: the global scaling factor, the heterotrophic respiration model, the CH_4:C temperature-dependence parameter (q_{10}), and the wetland-extent parameterization. In this study, all selected configurations use a global scaling factor of 166 Tg CH_4 yr^{-1} and the CARDAMOM heterotrophic respiration model. The ensembles differ in their specifications of CH_4: C temperature dependence (q_{10} = 3 in the "-3" series; q_{10} = 1 in the "-4" series) and in the wetland-extent parameterization (either precipitation-based inundation fields combined with GLWD or GLOBCOVER static maps). These combinations allow exploring how uncertainties in temperature sensitivity and wetland extent influence CH_4 flux estimates. The temporal resolution is monthly, with a spatial resolution of 0.5° x 0.5°.

Together, these three different approaches for CH_4 wetland emissions -Kaplan, CAMS-Inversion, and WetCHARTs ensembles -were integrated into WRF-GHG to estimate the "$CH_{4,WET}$" (equation 3) component of the model's biogenic CH_4 fluxes. Using multiple inventories allows the model to capture the diversity of plausible wetland emission estimates. For a more detailed description of the pre-processing methods for CH_4 anthropogenic, fire, and biogenic emissions in our simulations, please refer to Appendix A.

3.3.4 Biogenic CO_2 Fluxes - JULES Land Surface Model

The Joint UK Land Environment Simulator (JULES, Best et al., 2011) was used to simulate terrestrial biogenic carbon fluxes, providing an independent estimate of land–atmosphere CO_2 exchanges for comparison with the VPRM-based fluxes used in WRF-GHG. JULES is a process-based land surface model that represents energy, water, and carbon exchanges between the land surface and the atmosphere, including photosynthesis, autotrophic and heterotrophic respiration, and soil hydrology (Clark et al., 2011). The version utilized to run JULES was 7.0, based on nine plant functional types (PFT), including tropical forests (Harper et al., 2016). The model was run offline, not over a spatial area, but rather at a specific coordinate point (ATTO site) to simulate the corresponding conditions each hour, driven by hourly meteorological forcing derived from WRF outputs (T, RH, wind velocity, specific humidity, air pressure, rainfall, downward flux of short and long-wave radiation). JULES parameters were optimized for different sites within the Amazon biome, including the ATTO tower, as described in Prudente Junior et al. (2025). The simulated NEE was directly compared with the CO_2 fluxes from WRF-GHG at the ATTO, allowing an assessment of the sensitivity of WRF-GHG simulations to the choice of land surface biogeochemical model.

https://doi.org/10.5194/egusphere-2026-979
Preprint. Discussion started: 10 April 2026

4 Model Evaluation Approach

To assess the performance of the WRF-GHG model in reproducing CO_2 and CH_4 mole fractions, we first evaluated the simulated meteorological variables against observations, since local meteorological conditions strongly influence both GHG transport and surface fluxes. Simulated CO_2 and CH_4 and meteorological parameters were extracted at the grid points nearest to the ATTO Tower, ATTO-Campina site, INMET meteorological stations, and along the RF15 trajectory. A complete sensitivity analysis of the model using the INMET stations is provided in the supplementary material (Section A). For datasets with vertical resolution (ATTO and INSTANT Tower, ATTO-Campina, and RF15), simulated values were vertically interpolated linearly in height to match observed heights. All meteorological comparisons were performed at hourly resolution. For precipitation, we used the Integrated Multi-satellitE Retrievals for the global precipitation measurement (GPM) mission (IMERG), see Huffman et al. (2019). Simulated precipitation was computed by summing the "Accumulated total cumulus precipitation (RAIN)" and "Accumulated total grid-scale precipitation (RAINNC)" fields. These fields were aggregated to obtain daily totals (from 00:00 to 23:00 LT), and model output was spatially remapped to match the satellite resolution for consistent comparison. WRF-GHG internally converts fluxes from offline emission inventories into atmospheric concentration timeseries and adds to tracer variables representing the biogenic (BIO), biomass burning (BBU), and anthropogenic (ANTHRO) sources. The background tracer (BCK) is treated differently: it is not derived from fluxes but is prescribed directly in units of concentration (ppm) and is transported by the model without requiring a flux-to-concentration conversion. To compare observed and simulated GHG concentrations, model outputs underwent a numerical post-processing step in which total CO_2 and CH_4 concentrations were computed as:

$$CO_{2,total} = CO_{2,BIO-VPRM} + CO_{2,BBU} + CO_{2,ANTHRO} + CO_{2,BCK} \quad (1)$$

$$CH_{4,total} = CH_{4,BIO} + CH_{4,BBU} + CH_{4,ANTHRO} + CH_{4,BCK} \quad (2)$$

Here, $CO_{2,total}$ and $CH_{4,total}$ represent the total atmospheric concentrations of CO_2 and CH_4. The subindices $ANTHRO$ and BBU for both gasses refer to their anthropogenic and biomass burning components, respectively. $CO_{2,BIO-VPRM}$ corresponds to the biogenic CO_2 component estimated with the Vegetation Photosynthesis and Respiration Model. For methane, the biogenic component $CH_{4,BIO}$ includes contributions from wetlands, termites, and soil uptake:

$$CH_{4,BIO} = CH_{4,WET} + CH_{4,TERM} + CH_{4,Soil} \quad (3)$$

In this study, $CH_{4,WET}$ represents wetland emissions derived from three distinct inventories as mentioned in section 3.3.3. In order to evaluate the model's performance, we used several standard metrics of comparison (see Appendix B).

https://doi.org/10.5194/egusphere-2026-979
Preprint. Discussion started: 10 April 2026

5 Results and discussion

5.1 Evaluation of Simulated Meteorological Fields

Overall, the model reproduces the local meteorological conditions at ATTO reasonably well, particularly the diurnal cycle (Fig. 2). The simulated air temperature at 81 meters agrees closely with observations (MB = 0.58 °C; RMSE = 1.53 °C; r = 0.77), reproducing both the diurnal variability and the synoptic-scale fluctuations. In contrast, wind speed at 81 m shows larger deviations: wind speed exhibits a positive mean bias of 1.28 m s^{-1} (Fig. 2, top-right), and wind direction differences of -26.69° (Fig. S3). The positive mean bias in surface wind is often due to imperfect surface processes and topographic resolution. In particular, the dense vegetation and complex surface roughness of the Amazon forest can lead to inaccuracies in simulating wind flow and turbulence, especially at lower altitudes. Such discrepancies may introduce uncertainties in horizontal transport and consequently affect the modeled representation of CO_2 and CH_4 plumes as we will show in session 5.2.2.

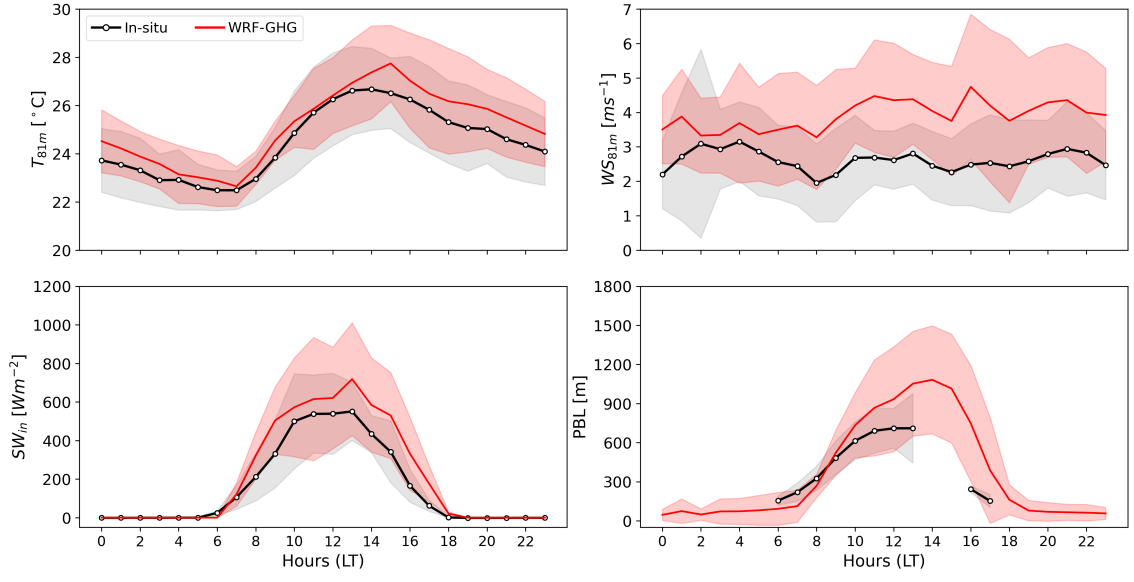

Figure 2. Mean diurnal variation of Temperature (T_{81m}) and Wind Speed (W_{81m}) at 81 meters; radiation, and the PBL height at INSTANT tower. Black circles indicate observations and red lines represent the simulated data. Average of the days from January 11 to 30, 2023.

The lower panels of Fig. 2 illustrate the model performance for shortwave (SW) radiation and PBL height. The model captures the timing and amplitude of the diurnal cycle of incoming SW radiation with a strong correlation (r=0.83), although peak values tend to be overestimated. This bias likely reflects deficiencies in cloud or convection parameterizations, a known challenge in tropical regions (Adams et al., 2009; Sakaguchi et al., 2018). The radiation overestimation propagates into the PBL evolution: WRF-GHG consistently predicts deeper daytime PBL heights (MB = 93.74 m; RMSE = 341.38 m; r = 0.61). Such differences in PBL growth directly influence vertical mixing and the dilution of GHGs, potentially contributing to mismatches between modeled and observed tracer concentrations. For example, a deeper PBL can dilute near-surface CO_2 and

https://doi.org/10.5194/egusphere-2026-979
Preprint. Discussion started: 10 April 2026

CH_4 concentrations, while timing errors in the convective boundary layer development may alter the dispersion and transport pathways of GHG plumes.

To further understand how meteorological uncertainties propagate into the simulated GHG fields, it is also important to examine additional processes that modulate surface fluxes and vertical transport, particularly precipitation and the vertical atmospheric structure. Fig. S5 shows that WRF-GHG reproduces the timing of rainfall events at ATTO, but tends to overestimate precipitation intensity, particularly during convective episodes (e.g., January 18, 24, 29). The rainfall spatial patterns shown in Fig. S6 reveals an overestimation in northwestern Amazonia while underestimating it in other regions. These biases are consistent with known challenges associated with representing tropical convection in regional models (Sousa et al., 2019; Hernández et al., 2024). These challenges are often related to the limitations of regional models in accurately capturing sub-grid-scale turbulent processes, such as deep convection, cloud formation, and the heat and moisture fluxes occurring in the lower layers of the atmosphere. The representation of clouds, in particular, remains a significant issue, as cloud models or cumulus parameterizations operates within the grey zone of convection, where key aspects of cloud dynamics and convective processes cannot be fully resolved which are crucial for accurate precipitation and wind forecasts. To address this, the WRF model's cumulus parameterization was disabled for the 6 km nested domain (see Table 2), which falls within the grey zone. This approach allows for a more explicit representation of convection, improving the resolution of small-scale processes and enhancing the accuracy of precipitation and convection forecasts.

To assess the vertical atmospheric structure, radiosonde data from the ATTO-Campina station were compared with WRF-GHG simulations (Fig. S7). The model reproduces the vertical profiles of potential temperature and specific humidity reasonably well at both 10:00 LT and 16:00 LT, with high correlations ($r \approx 0.98$–0.99). These results indicate that the model captures the main thermodynamic structure of the lower troposphere, including morning stability and afternoon boundary layer deepening. In contrast, larger discrepancies are observed in the wind speed profiles, particularly within the boundary layer, where WRF-GHG exhibits an overestimation in the morning (deviation = 0.44 m s^{-1} at 10:00 LT) and even larger deviations in the afternoon (deviation = 0.79 m s^{-1} at 16:00 LT). Similar discrepancies were also reported in Beck et al. (2012). These wind-related errors suggest a model limitation representing momentum mixing in the boundary layer and the transition from calm morning conditions to afternoon convective turbulence. Such biases likely arise because the model underestimates surface rugosity, which in turn affects plume lift, drag, and the overall transport of greenhouse gases, occur under conditions dominated by surface convection or strong vertical wind shear.

To complement the radiosonde-based evaluation and extend the assessment into the free troposphere, we also used observations from the CAFE-Brazil aircraft campaign to validate WRF-GHG along the flight trajectories of 14 January 2023 (see Fig. 3). Aircraft observations were aggregated to 10-min averages to reduce noise and facilitate comparison to the instantaneous hourly WRF-GHG outputs. Aircraft observations matching with each instantaneous hourly model output were compared. In general, instantaneous hourly comparisons demonstrate strong performance, particularly for potential temperature (r = 0.99 and MB = -0.90 K) and specific humidity (r = 0.98 and MB = 0.93 g kg^{-1}) (Table S3). Wind speed is also reasonably well rep-

https://doi.org/10.5194/egusphere-2026-979
Preprint. Discussion started: 10 April 2026

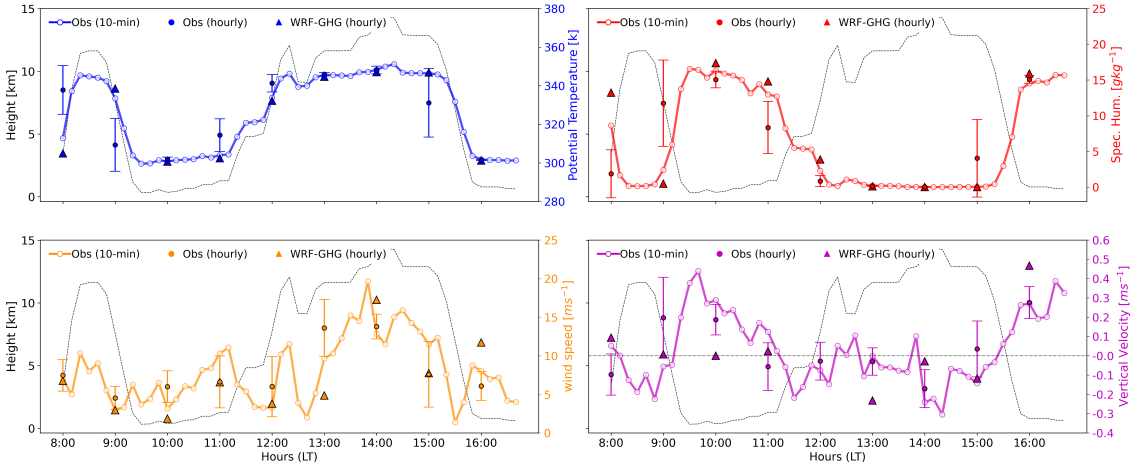

Figure 3. Validation of WRF-GHG simulations using aircraft observations from the CAFE-Brazil campaign on 14 January 2023 for the variables: Potential temperature (blue, right axis); specific humidity (red, right axis); Wind speed (orange, right axis); Vertical wind velocity (purple, right axis). Solid lines and open circles represent 10-minute averages from observations, filled circles are hourly averages from observations, and triangles are simulated values. The gray dashed line in all panels indicates the aircraft height. Aircraft observations were averaged into 10-minute intervals to reduce noise and facilitate comparison. In contrast, the WRF-GHG outputs are available hourly.

resented, with correlation of 0.75 and RMSE of 3.08. While the model captures high wind conditions fairly well, deficiencies in simulated surface winds are attributed to local influences that are not well represented in the model, rather than to errors in the synoptic-scale flow. In contrast, vertical velocity exhibits very weak correlation (r = -0.11) and small mean bias (0.40 m s^{-1}), indicating limited model skill in capturing small-scale vertical motions. These quantitative results confirm that WRF-GHG reproduces the large-scale vertical gradients and thermodynamic structure of the free troposphere, particularly temperature and humidity, but struggles with variables sensitive to transient or unresolved processes. The poor performance in vertical velocity is consistent with known limitations in convective parameterization, which do not explicitly resolve cloud convection, relying on parameterized vertical mixing. However, it is clear that the main differences between observed and simulated occurs when the airplane is flying in lower altitude, showing the importance in improving surface-atmosphere interaction in the numerical models over Amazonia.

In summary, WRF-GHG performs well in capturing temperature, humidity, radiation, and boundary-layer evolution, but systematic biases in winds, convection, and precipitation introduce uncertainties in atmospheric transport. Because these processes directly control the mixing, dilution, and advection of trace gases, the meteorological limitations identified here provide important context for understanding the behavior of the CO_2 and CH_4 tracers. The next subsection examines how these transport-related uncertainties impact the simulated GHG fields.

https://doi.org/10.5194/egusphere-2026-979
Preprint. Discussion started: 10 April 2026

5.2 Performance of WRF-GHG Tracer Simulations Against In-situ Observations

5.2.1 CO_2 simulations

Figure 4 presents the hourly time series and mean diurnal cycle of measured total CO_2 concentrations (top panels) and fluxes (bottom panels) at the INSTANT Tower at 81 meters, compared with WRF-GHG simulations using two configurations of the VPRM module: the default version (VPRM-default; blue) and the regionally calibrated version (VPRM-cal; red). VPRM parameters were optimized by Botía et al. (2025a) (parameters listed in Table S4, supplementary material), resulting in improved representation of temporal variability in CO_2 concentrations. With this calibration, the mean model–observation difference decreased from -16.62 ppm to -1.60 ppm, while maintaining a similar moderate correlation (r = 0.59). Notably, VPRM-cal better captures the nighttime accumulation and daytime drawdown driven by photosynthesis, whereas VPRM-default continues to underestimate both nighttime buildup and daytime mixing ratios (Fig. 4). The effect of VPRM calibration impacts not only the concentration baseline, but also the diurnal amplitude of CO_2 concentrations. The amplitudes estimated by VPRM-cal are closer to the observations. Multiple studies (Seo et al., 2023; Mai et al., 2023; Park et al., 2018; Wu et al., 2020) have demonstrated that calibrating VPRM parameters for the region of interest is essential for accurately representing ecosystem CO_2 fluxes. The default VPRM parameters were originally developed for European ecosystems, which differ substantially from Amazonian vegetation in terms of physiology, phenology, and environmental drivers. However, discrepancies between observations and CO_2 concentration simulations cannot be attributed solely to surface CO_2 fluxes. As discussed in Section 5.1, meteorological factors such as PBL height, wind speed, and solar radiation impact near-surface CO_2 mixing. Overestimating PBL depth can dilute CO_2 concentrations during the day, while nighttime mixing biases may reduce CO_2 buildup. Similarly, inaccuracies in shortwave radiation affect photosynthesis rates, which in turn influence the daily cycle of CO_2 uptake and release. These meteorological limitations contribute to the observed concentration errors in both VPRM configurations.

The diurnal cycle on the right side of Fig. 4 also reveals a characteristic early-morning "flushing peak" in the measured CO_2 concentrations, corresponding to the rapid release of CO_2 accumulated overnight under the canopy (de Araújo A., 2008). However, WRF-GHG simulates this peak with a lag of approximately one hour, suggesting that the model does not fully capture the dynamics of nighttime CO_2 accumulation or its release at dawn (see Fig. 5). This lag is more pronounced at lower altitudes (24 m and 38 m), where the model tends to underestimate the morning peak. This discrepancy likely reflects the sensitivity of CO_2 dynamics to factors such as canopy structure, the onset of turbulence, and near-surface stability in Amazonian forests. The data in Fig. 5 emphasize this limitation, showing a morning discharge peak similar to that observed at 24 m, but with a distinct lag in the model's simulation. At higher altitudes (81 m), the model better represents CO_2 concentrations, suggesting that vertical mixing processes are better captured above the canopy. This comparison highlights the importance of accurately representing vertical stratification in Earth-atmosphere models, especially to correctly simulate the dynamics of nighttime CO_2 accumulation and its morning release in the lower canopy, where these processes are more pronounced.

The lower panels of Fig. 4 represent simulated net ecosystem exchange (NEE), where negative values indicate daytime carbon uptake and positive values correspond to nighttime respiration. NEE is computed as the difference between GPP and

https://doi.org/10.5194/egusphere-2026-979
Preprint. Discussion started: 10 April 2026

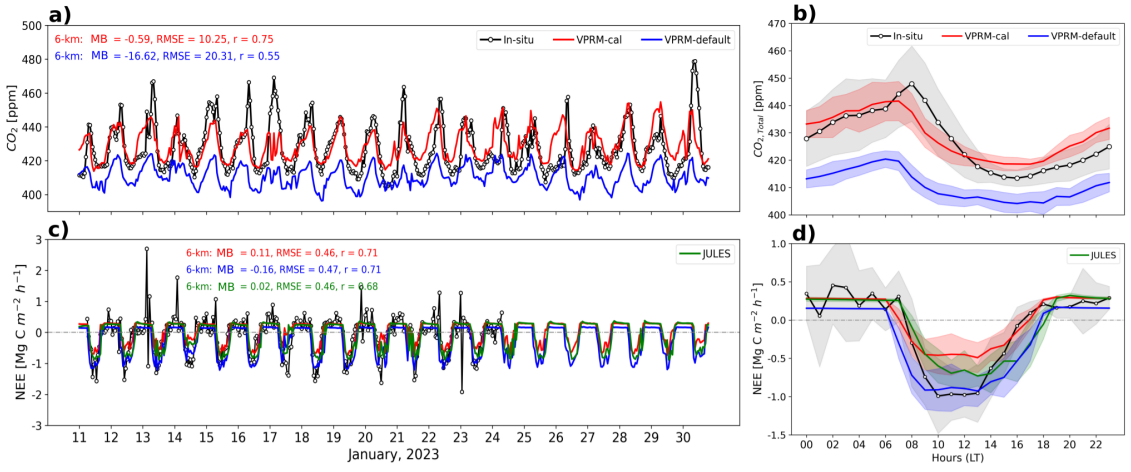

Figure 4. (a) Time series of observed and simulated total carbon dioxide (CO_2) concentrations at 81 m, and (c) net ecosystem exchange (NEE), at the INSTANT tower for January 2023. (b) Mean diurnal variation of total CO_2 concentration at 81 m and (d) NEE at INSTANT Tower. Black circles denote in-situ observations. Red and blue lines show WRF-GHG simulations using the calibrated (VPRM-cal) and default (VPRM-default) VPRM modules, respectively. The green line represents simulations using the JULES land surface model. Shaded areas indicate the variability ($\pm$ 1 standard deviation) of observations and model simulations.

ecosystem respiration (Res) using the VPRM-WRF module (blue and red lines) and the JULES model (green line). Compared to the observations at ATTO, VPRM-cal and JULES underestimated the diurnal carbon sink, although they correctly reproduced the magnitude of nighttime respiration. However, VPRM-default underestimated nighttime respiration. Comparing the three carbon flux modeling approaches, JULES showed the best performance, despite the underestimation in the diurnal carbon uptake, possibly caused by limitations in the representation of canopy conductance, soil respiration dynamics, or carbon allocation under Amazonian conditions. Optimization of the parameters of the JULES model for the ATTO site Prudente Junior et al. (2025) may have contributed to decreasing the bias against observations. This highlights the importance of site-specific tuning of model parameters. Although VPRM-cal used calibrated parameters for the Amazon forest, they were not specific for the ATTO site.

Connecting CO_2 fluxes and concentrations, note that VPRM-cal underestimated the daytime carbon uptake (Fig. 4c), resulting in higher CO_2 concentrations compared to VRPM-default (Fig. 4a), and in lower biases compared to observations at ATTO. In addition, bias in the modeled CO_2 background may exert an influence on modeled concentrations. Model-observation mismatches at tower sites through combined effects of measurement instrument biases, meteorological transport model uncertainties and background, contribute to regional flux estimate uncertainties of approximately 10-30% (Masarie et al., 2011; Botía et al., 2020; Gerken et al., 2021; Miles et al., 2021), which are particularly pronounced at tall towers like ATTO, where complex atmospheric transport and decoupling between local and regional signals complicate accurate background determination.

https://doi.org/10.5194/egusphere-2026-979
Preprint. Discussion started: 10 April 2026

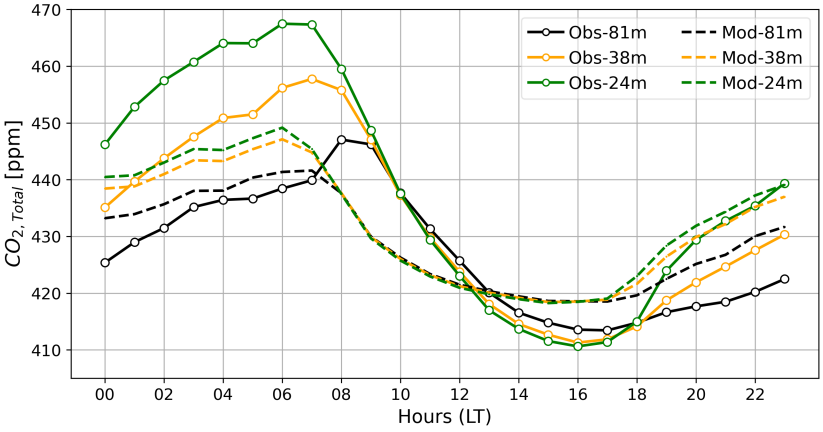

Figure 5. Diurnal cycle of CO_2 concentration at different altitudes from January 11 to 30, 2023. Observations (solid lines) and WRF-GHG model (dashed lines) for CO_2 levels at 81m (black), 38m (orange), and 24m (green).

There are important structural differences between the VPRM and JULES models. VPRM relies on empirically calibrated relationships between vegetation indices, radiation, and temperature, enabling it to capture site-specific flux variability when properly tuned. VPRM was made to be a simple diagnostic model, proving first guess estimates for biogenic CO_2 exchanges within atmospheric regional transport models. In contrast, JULES explicitly represents photosynthesis, respiration, and soil processes, which enhances physical consistency, but may dampen short-term variability associated with rapid canopy responses and turbulence-driven fluxes. The comparison of modeled CO_2 fluxes against observations at the ATTO site provides an uncertainty measure to the regional flux estimates, when the models are applied to the whole Amazon Basin. Specifically, when using the WRF-GHG model with the given configurations, the simulated NEE for the ATTO region may be overestimated by up to 16% (VPRM-default), 11% (VPRM-cal), and 2% (JULES).

5.2.2 For CH_4 simulations

Figures 6 and S11 (from supplementary material) display the total observed (black line with open circles) and simulated CH_4 concentrations at ATTO for January 2023. The simulated CH_4 total concentrations were dominated by the background (95 %) and by the biogenic component (4 %). In-situ data show a nearly constant concentration along the day, with a similar concentration to the simulated background, driven by the variability of simulated wetland CH_4 mixing ratios (Figure S12). This result occurs because the ATTO plateau has no strong sources, and the simulated diurnal cycle is not associated with biogenic emissions but with incorrect transport. All simulations overestimated the observed CH_4, with CAMS-Inversion (blue triangles) providing the best agreement, showing the lowest mean bias compared to the other inventories. Kaplan (red stars) consistently produced concentrations exceeding 2100 ppb, likely due to an overestimation of wetland emissions (Fig. S12). This aligns with Beck et al. (2013), who reported an average 76% overestimation in wetland emissions using the Kaplan model, which likely

https://doi.org/10.5194/egusphere-2026-979
Preprint. Discussion started: 10 April 2026

contributed to the higher CH_4 concentrations in these simulations.

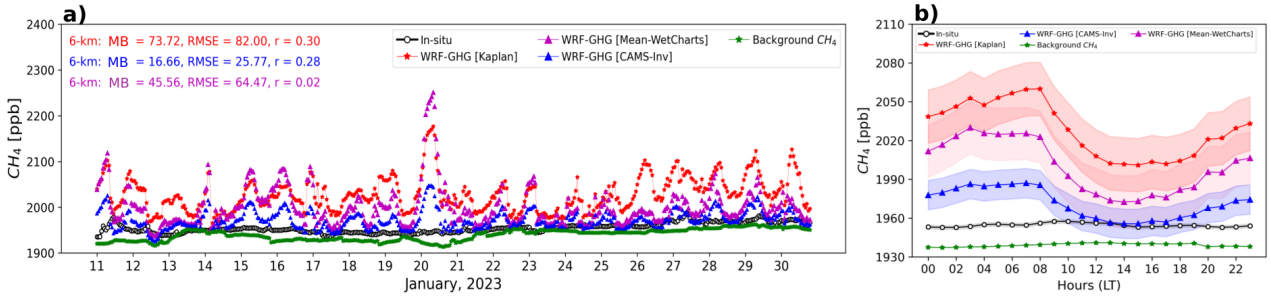

Figure 6. (a) Time series and (b) mean diurnal cycle of total CH_4 concentration at INSTANT tower during January 2023, comparing observations (black circles) with simulations using Kaplan (red stars), WetCHARTs ensemble (magenta triangles) and CAMS-Inversion (blue triangles) wetland fluxes and the background (green line) field. All comparisons correspond to measurements at 81 meters above ground level.

The marked diurnal cycle of simulated CH_4 concentrations is driven by atmospheric transport and PBL processes in the model, rather than by emission dynamics. While the Kaplan module responds to dynamic model variables, CAMS-Inversion and WetCHARTs consist of monthly CH_4 flux data, constant at the hourly scale. The three modeling approaches show diurnal cycles correlated with each other, suggesting that PBL processes and advection may drive this diurnal variability. The simulated mean diurnal cycles of CH_4 concentrations show the typical pattern of nighttime accumulation and daytime dilution, controlled by boundary-layer dynamics (Tóta et al., 2012; Beck et al., 2012; Miller et al., 2007). Diurnal variability of the advective transport simulated by the model may also contribute to the simulated temporal variability (Botía et al., 2020; Querino et al., 2011).

Discrepancies between observed and simulated CH_4 mole fractions may also have a contribution of the simulated wind field. The model predicts predominantly northeasterly winds and larger wind speeds (Fig. S14, upper panels), whereas observations indicate prevailing winds from northeast-east and lower wind speeds. This bias directly affects CH_4 transport. For example, the simulated CH_4 enhancement on 20 January reaches $\approx$ 2200 ppb (Fig. 6). In this day, the model misrepresented the local wind direction at ATTO, predicting winds mostly from the southeast while observations showed a more variable wind direction, ranging from east to southwest (Fig. S14). A section of the Amazon River is located southeast of ATTO, about 150 km away, see Fig. S13 and Fig. 7. The river and its flooded area is a source of CH_4 in the model, therefore, the simulated advection of CH_4 likely contributed to the modeled concentration increase on January 20th. However, as discussed in Botía et al. (2020), the Amazon was discarded as a primary CH_4 source for nighttime positive gradients due to wind speeds below 5 m/s, which limited transport to ATTO. In contrast, the WRF-GHG model sometimes simulates winds above 5 m/s (Fig. S14), allowing CH_4 advection from the Amazon, suggesting it could be a relevant source in certain conditions. This highlights key

https://doi.org/10.5194/egusphere-2026-979
Preprint. Discussion started: 10 April 2026

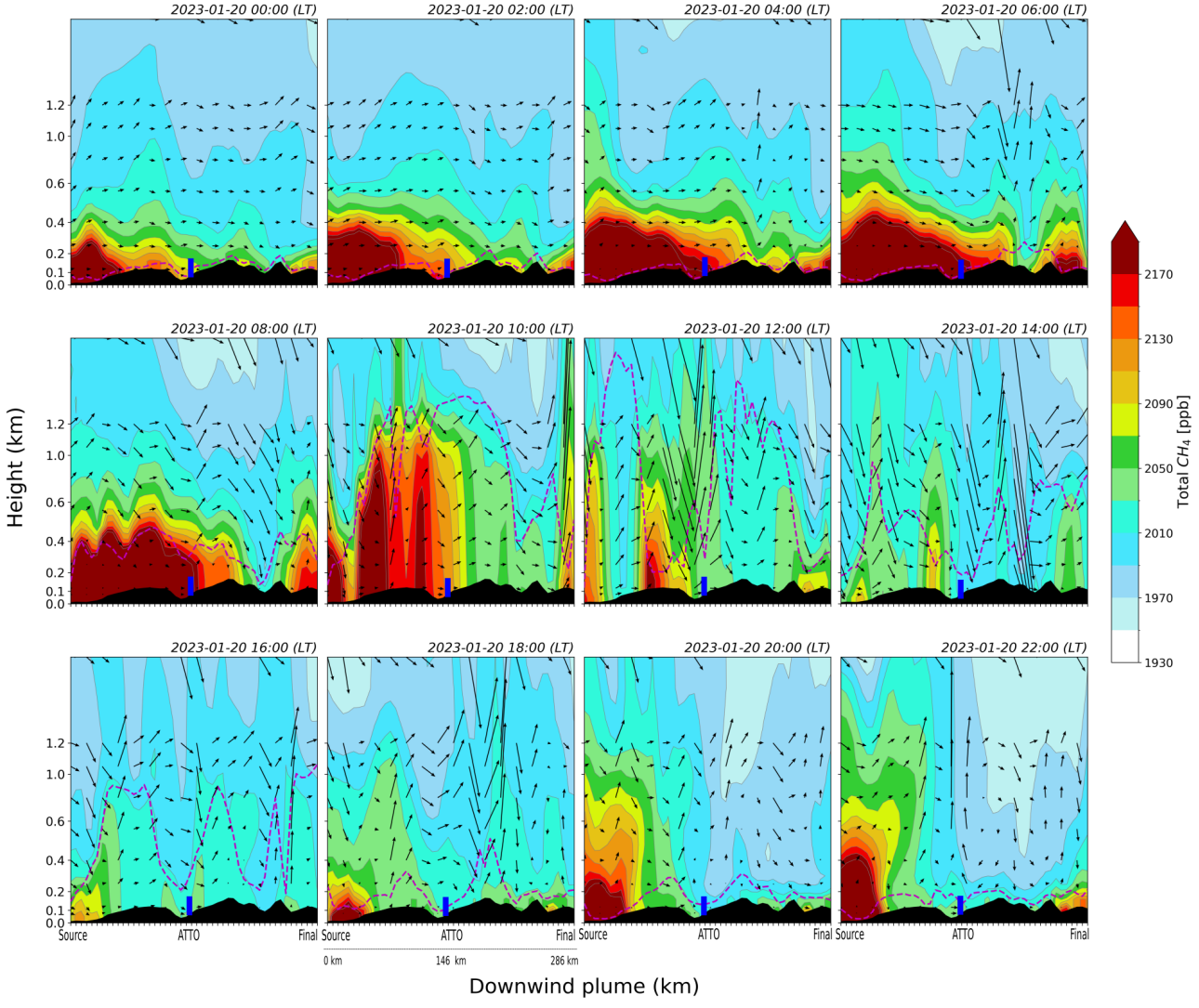

Figure 7. Vertical cross-sections of simulated total CH_4 concentrations (color shading) and wind vectors along the downwind plume at the ATTO site on 20 January 2023, following the path of the line drawn between the Amazon River and ATTO (see Fig. S13a). Simulated CH_4 concentrations are based on the Kaplan model. Wind vectors are represented by black arrows, the planetary boundary layer (PBL) is highlighted by the magenta dashed line, and the topography is shown in black. The Blue rectangle correspond to ATTO site, the word "Source" represent the Amazon river and word "Final" indicates a point near Balbina Lake.

differences between observed and simulated wind patterns.

To further investigate the contribution of advection to the CH_4 modeled concentrations at ATTO, vertical cross sections of concentrations and winds were depicted in Fig. 7 for January 20th, showing a transect from the Amazon River towards the

https://doi.org/10.5194/egusphere-2026-979
Preprint. Discussion started: 10 April 2026

ATTO site. Elevated CH_4 concentrations remain largely confined to the lower 0.5–1.5 km throughout the day, reflecting strong boundary-layer. Before dawn (00:00–06:00 LT), weak winds and a shallow, stable surface boundary layer favor near-surface accumulation, forming a dense CH_4-rich layer near the emission source. As solar heating develops (08:00–14:00 LT), the convective layer deepens and mixing intensifies, redistributing CH_4 vertically and intermittently transporting higher-concentration air masses to 1–1.5 km (≈ 8:00 LT). In the afternoon and evening (16:00–22:00 LT), partial re-stabilization of the lower atmosphere leads to renewed near-surface accumulation as vertical mixing decreases.

A notable feature of this simulation is the persistent northwest-to-southeast advection pattern, which directs the wetland plume toward ATTO throughout the day (Fig. S15). This pattern reflects the model's low-level wind bias and explains the pronounced simulated CH_4 increase at the tower, despite observations indicating that winds flow from different direction. Cross-sections demonstrate how errors in low-level wind direction and convective boundary-layer depth can propagate into significant biases in CH_4 transport and vertical distribution, highlighting that meteorological uncertainties, rather than emissions variability, dominate the discrepancies between simulated and observed concentrations during this event. Figure S13 further confirms this poor representation of methane concentrations at the ATTO tower, revealing how the modeled advection of biogenic methane concentrations leads to overestimated CH_4 levels at the site.

This does not means that the CH_4 fluxes and background are correctly represented by the simulations, the magnitude of the fluxes and their spatial distribution may not be well represented. The simulated spatial distribution of CH_4 concentration may be incorrectly represented as we will discuss in the next section.

5.3 Comparison of Simulated CH_4 with Aircraft Measurements

Figure 8A shows the spatial distribution of CH_4 total concentration at 81 meters, averaged for the period of the RF15 mission in January 14, 2023 (8-16 LT), simulated using the Kaplan model. Hotspots of CH_4 concentrations were simulated along Negro, Solimões and Amazon Rivers. Hotspots of CH_4 concentrations were simulated along the Negro, Solimões, and Amazon rivers, as well as near areas known as '*campinarana*' (forests on white-sand soils; in T5) (Botía et al., 2020; de Oliveira et la., 2022). Figure 8B presents a comparison between CH_4 simulations and observations from aircraft in January 14, 2023. To make this comparison, the CH_4 concentration data from the WRF-GHG model and the aircraft measurements are first spatially and temporally aligned. Due to differences in temporal resolution, the aircraft data was averaged over 10-minute intervals and then the nearest hourly data were selected for comparison with the model. The comparison was conducted at different altitudes along the flight trajectory, between 08:00 LT and 16:00 LT. The simulated CH_4 concentrations reasonably reproduce both the spatial distribution of observed CH_4, including the observed changes in methane levels as function of the airplane altitude (Fig. 8, panel B).

Among the different wetland emission inventories, the simulation using WetCHARTs emissions shows the best agreement with the observed data (r = 0.50; MB = -27.1 ppb; RMSE = 92.6 ppb), capturing both the magnitude and the spatial variability

https://doi.org/10.5194/egusphere-2026-979
Preprint. Discussion started: 10 April 2026

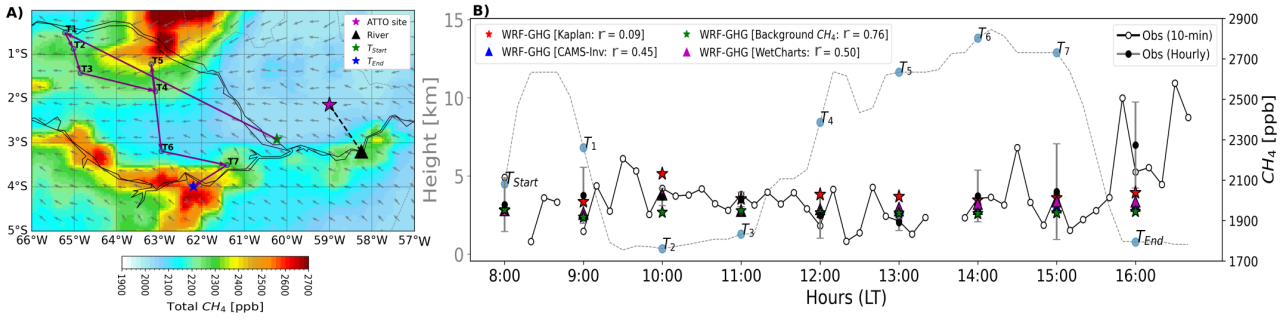

Figure 8. Panel A: Shows the spatial distribution of total methane (CH_4) concentrations over the region where the RF15 occurred on January 14, 2023, simulated using the Kaplan model. The star marks the location of the ATTO (Amazon Tall Tower Observatory), while the black triangle represents a sector of the Amazon River, about 150 km southeast ATTO. The markers "Tstart, T1, T2, T3, … T6, Tend" indicate the aircraft's position at specific time points between 08:00 and 16:00 LT. Panel B: Displays the temporal variability of CH_4 concentrations, comparing the observed data with simulations from the WRF-GHG model, considering three different wetland emission inventories. The simulated CH_4 data represent instantaneous hourly values, while the observed data are recorded every 10 minutes. The comparison between the simulated and observed data was made by matching the simulated hourly values. The error bars represent the variability of CH_4 concentrations within the hourly average. The gray dashed line represents the altitude along the flight trajectory.

of CH_4. Simulations based on CAMS-Inversion also show a reasonable agreement with the observed values (r = 0.45; MB = -38.2; RMSE = 97.9). In contrast, the Kaplan emission model yields poorer results, with the simulated CH_4 concentrations overestimating the observed values (r = 0.09; MB = 19.9 ppb). This discrepancy was already observed in the CH_4 analysis at 81 meters above the ATTO site, where simulations using the Kaplan inventory produces abnormally high CH_4 concentrations (see Fig. 6). The overestimation can be attributed to the Kaplan inventory's higher methane fluxes, which are based on a larger percentage of inundated areas. This leads to higher CH_4 emissions compared to the other inventories. The simulated background CH_4 concentration component remains nearly constant along the flight path, confirming that the observed CH_4 has reduced vertical stratification and above the boundary layer, the concentration is homogeneous. A key observation is that the background CH_4 concentration dominates along most of the flight trajectory. Flights where surface emission effects are most evident is between T2 and T3, when the aircraft flies lower and appears to cross a region with elevated CH_4 concentrations. At T2 and T3, the background CH_4 concentration is lower than the observed concentrations, indicating that emission inventories must be considered in these regions to accurately reproduce the observed data. The aircraft passes near a significant CH_4 emission hotspot, known as *campinarana* (T4 and T5). While the observed CH_4 concentrations above the boundary layer remained constant, the simulated concentrations, based on the Kaplan inventory, overestimated the observed data. This discrepancy is directly attributed to the wetland map used (see Fig. 8, panel C; paths T4 and T5). In contrast, at other points along the trajectory, far from emission hotspots, the background concentration is well represented by the model.

https://doi.org/10.5194/egusphere-2026-979
Preprint. Discussion started: 10 April 2026

To investigate the contribution of different CH_4 tracers to the total concentration along the aircraft trajectory, we analyzed the simulated background (Fig. 9, panel F) and biogenic wetland components separately (Fig. 9, panel C, D and E). Panels C, D, E and F show the vertical distribution of simulated CH_4 concentrations (in ppb) from the WRF-GHG model along the aircraft trajectory during the RF15 mission on January 14, 2023. Figures 9 (C-F) display CH_4 concentrations across different heights from 0 to 14.7 km and span various time intervals between 08:00 and 16:00 LT, with data points marked as "Tstart, T1, T2, T3, … T6, Tend". In Panel C, the simulation using the Kaplan emission inventory reveals high CH_4 concentrations near surface, particularly during time segments from T1 to T4. The CH_4 plume appears most concentrated close to the flight trajectory near wetland regions (as shown in Fig. 8 panel A). This panel also shows significant vertical variation in the CH_4 concentration, suggesting an overestimation of near-surface CH_4 levels in the Kaplan simulation, especially during the morning hours when the boundary layer is more stable. The wind direction, shown by the black vectors, transport CH_4 downwind along the flight, with concentrations decreasing slightly as the aircraft moves away from the river region.

In Panel D, the simulation using the CAMS-Inversion emission inventory shows a similar general trend, but with slightly lower CH_4 concentrations compared to the Kaplan inventory. As the inventory does not impact the model dynamics, all panels should have the same patterns, with the difference in the concentration, as the concentration are the difference among the emission inventory. These sources are responsible for the observed CH_4 increases, particularly in the areas near the wetland-dominated region. Panel E presents the simulation using the WetCHARTs emission inventory, which aligns most closely with the observed CH_4 concentrations. In this panel, CH_4 concentrations remain relatively consistent with the observed data across different altitudes, particularly in the lower to middle layers of the atmosphere. The temporal variation in CH_4 levels is also captured more accurately, as seen in the transition of concentrations between time segments T4 to T7. Both CAMS-Inversion and WetCHARTs simulation provide the best agreement with the observed CH_4 plume, demonstrating a more accurate representation of CH_4 fluxes from the wetland regions. This alignment is particularly evident when compared to aircraft trajectory shown in Fig. 8, panel B, where high concentrations are observed precisely along the aircraft trajectory, reinforcing the regional source of CH_4.

Overall, these panels demonstrate that the simulated CH_4 concentrations follow the expected pattern of downwind dispersion, with higher concentrations observed in the areas near the wetland-dominated regions. The consistency between the CAMS-Inversion and WetCHARTs inventories and the observed concentrations highlights their ability to capture the spatial distribution of CH_4 particularly in regions influenced by biogenic sources like wetlands. The wind direction also plays a crucial role in shaping the observed CH_4 plumes, as it transports CH_4 from the wetland regions downwind along the aircraft's trajectory. A notable section of the flight is between T2 and T3, where the aircraft flies closer to the surface. In this region, surface emissions become more significant, and the background CH_4 concentration has less influence.

https://doi.org/10.5194/egusphere-2026-979
Preprint. Discussion started: 10 April 2026

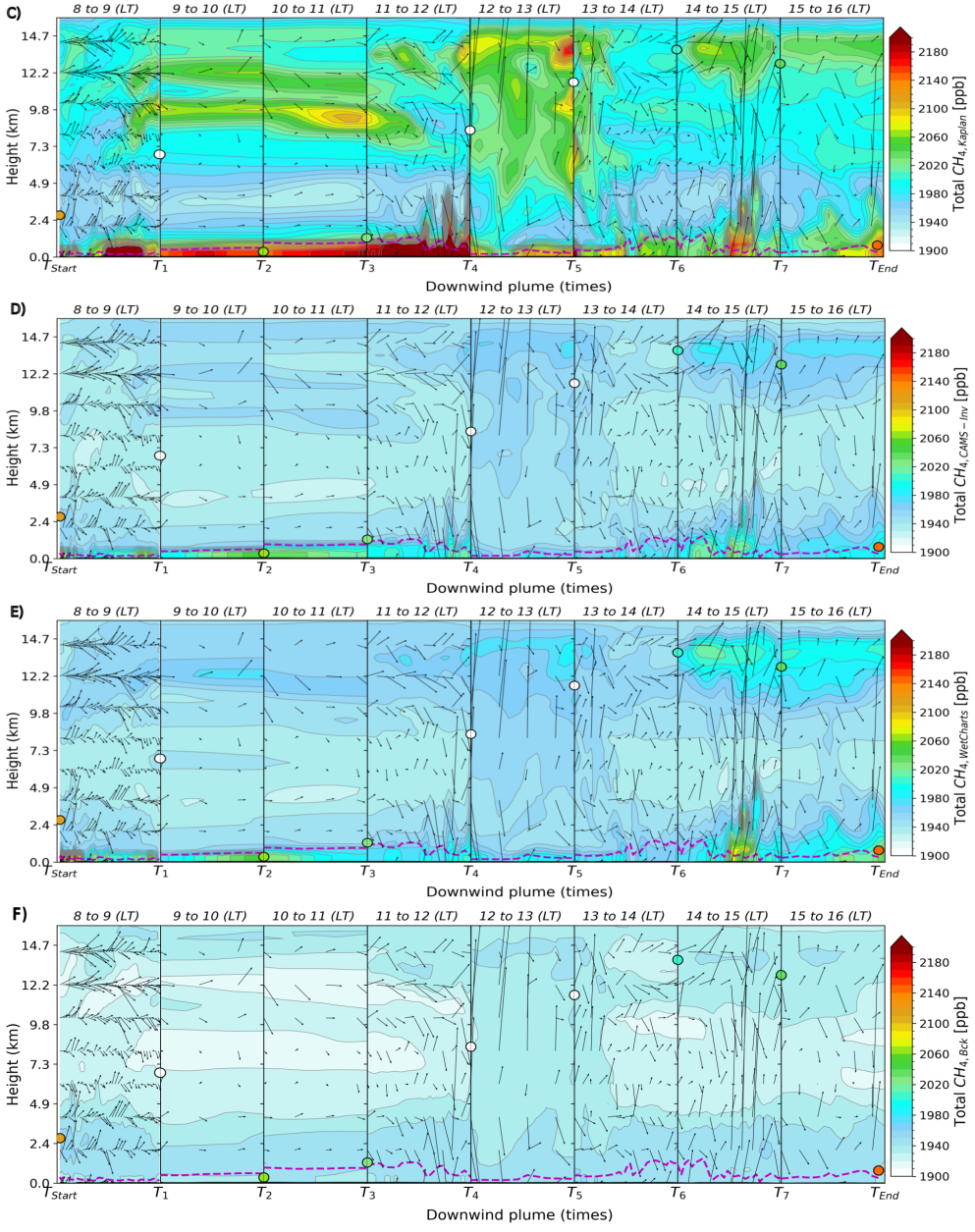

Figure 9. Continued from Figure 8. Vertical profiles of simulated CH_4 concentrations along the RF15 aircraft trajectory on January 14, 2023, using different wetland emission inventories (Kaplan, CAMS-Inversion and mean WetCHARTs). Panels C, D, and E show CH_4 concentrations at altitudes between 0 km and 14.7 km during different time intervals (08:00 to 16:00 LT). Panel F displays background CH_4 concentrations in the same altitude range and time intervals (08:00 to 16:00 LT). Wind vectors are indicated by black arrows and the planetary boundary layer (PBL) is shown by the dashed line in magenta. Aircraft measurements are represented by markers.

https://doi.org/10.5194/egusphere-2026-979
Preprint. Discussion started: 10 April 2026

6 Conclusions

WRF-GHG simulations of CO_2 and CH_4 fluxes and concentrations over the Amazon were evaluated against in situ and airborne measurements collected during the CAFE-Brazil campaign using different biospheric flux parameterizations and background datasets. In terms of meteorology, the model successfully reproduced the diurnal cycles of temperature, radiation, and humidity; however, systematic biases in wind speed and direction, precipitation, and planetary boundary layer (PBL) height were identified, directly affecting the transport and mixing of trace gases. In comparison to other studies in tropical regions, our results confirm ongoing challenges in accurately representing convective processes and local circulation in regional models, aligning with broader modeling efforts that emphasize the need for improved atmospheric transport representations. By combining tower and aircraft observations with multiple tracer configurations, this study provides a more comprehensive assessment of how transport and emission uncertainties interact across spatial scales, thus contributing valuable insights for future model improvements.

For CO_2, regional calibration of the VPRM biospheric flux module (VPRM-cal) substantially improved agreement with observations at ATTO, reducing the mean bias from -16.62 ppm to -1.60 ppm and yielding a more realistic carbon budget. Persistent discrepancies, particularly in the timing of the early-morning peak, highlight limitations in representing vertical stratification and near-surface turbulence. Comparisons with JULES showed consistent carbon flux magnitudes but differences in diurnal variability. Although JULES achieves higher accuracy when locally calibrated, VPRM-cal offers a good compromise between performance and computational efficiency. These results emphasize the importance of accurately representing the radiation field inside the canopy and the associated turbulence. Uncertainties in atmospheric transport, particularly in vertical mixing and radiation, can limit the accuracy of top-down CO_2 flux estimates, even when flux parameterizations are improved. These challenges, therefore, have important implications for the reliability of carbon budget estimates in tropical regions.

For CH_4, simulated concentrations were largely controlled by background concentration and atmospheric transport, with local emissions playing a secondary role at ATTO. The simulations produced an artificial diurnal cycle driven by PBL dynamics, in contrast to the nearly constant observed concentrations, highlighting deficiencies in the representation of boundary-layer transport (particularly horizontal mixing), which compromise the concentrations observed at ATTO. Among the flux models, Kaplan strongly overestimated CH_4, whereas CAMS-Inversion and WetCHARTs showed better agreement with both surface and aircraft observations. Aircraft observations from the CAFE-Brazil campaign further demonstrate that WetCHARTs and CAMS-Inversion better capture the spatial variability of CH_4. These results are consistent with other recent methane modeling studies, which also emphasize the need for better representation of atmospheric transport and wetland emissions in the Amazon.

Overall, these results underscore that meteorological uncertainties—particularly in PBL dynamics and the description of radiation within the understory—are a primary source of error in greenhouse gas simulations over the Amazon. Improving the representation of convection, vertical transport, and surface–atmosphere interactions, together with better-constrained bio-

https://doi.org/10.5194/egusphere-2026-979
Preprint. Discussion started: 10 April 2026

spheric flux models, is essential to enhance the reliability of regional carbon budget estimates. These implications suggest that further model improvements are critical for refining the accuracy of greenhouse gas fluxes in tropical forests and for more reliable future climate projections.

Appendix A: WRF-GHG-Prepy – Setup and Workflow

WRF-GHG-Prepy (https://github.com/rnoeliab/WRF-GHG-Prepy) is a Python-based preprocessing tool developed to integrate all relevant greenhouse gas (GHG) emissions inventories for use with the WRF-GHG modeling system. It facilitates the preparation of input datasets required for simulating GHG fluxes and atmospheric transport using the Weather Research and Forecasting (WRF) model, coupled with the Greenhouse Gases module (WRF-GHG).

WRF-GHG supports both online and offline treatments of emissions. Online flux models dynamically calculate biogenic and soil–atmosphere exchanges during model runtime, while offline inventories provide precomputed emissions from anthropogenic and biomass-burning sources that are introduced as surface or boundary fluxes. To obtain regional GHG emissions, we separated into background and regional contributions. Background contributions comes from sources outside the study domain and are transported into the region from other continents, whereas regional contributions originate within the study area and include anthropogenic emissions (excluding biomass burning), biomass burning, and biogenic sources such as wetlands, termites, and soil uptake.

To integrate these diverse emission sources within WRF-GHG, we developed WRF-GHG-Prepy as a unified preprocessing framework. The tool is structured into four main modules (Fig. A1): (I) biogenic emissions (named as "GHG module"), (II) biomass-burning emissions (named as "GFAS-Fires"), (III) anthropogenic emissions (named as "EDGAR-Anthro"), and (IV) initial and lateral boundary conditions (named as CAMS-Bck) for GHGs. Consolidating all emission components into a single preprocessor addresses the inherent complexity of handling heterogeneous datasets and formats. WRF-GHG-Prepy facilitates activation of the GHG module in WRF (chemical options 16 and 17; Beck et al. (2011)), thereby enhancing the model's capability to simulate regional and background GHG contributions in a consistent and reproducible manner.

A1 Summary of Setup and Execution Steps

The following procedural steps summarize the use of WRF-GHG-Prepy Version 1:

A2 Environment Setup

The user clones the repository and sets up the environment using the provided environment.yml file.

A3 WRF Input Preparation

Place required WRF model files (wrfinput, wrfbdy, and geo_em.d0#.nc) in the wrf_inputs/ directory

https://doi.org/10.5194/egusphere-2026-979
Preprint. Discussion started: 10 April 2026

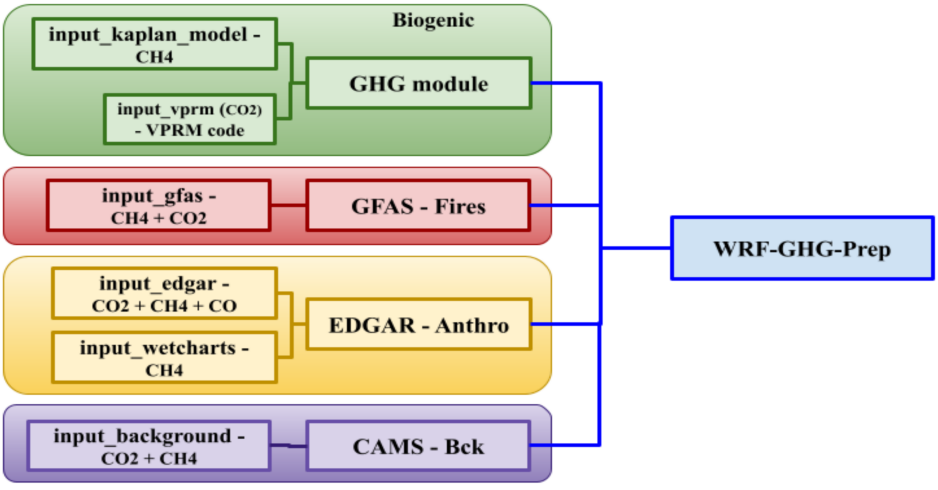

Figure A1. Workflow of WRF-GHG-Prepy Version 1 - (Source: https://github.com/rnoeliab/WRF-GHG-Prepy)

A4 Biogenic Emissions

A4.1 CO_2 via VPRM

Process MODIS and MapBiomas or Copernicus Land Cover data using the vprm_preprocessor_new.py script (from the pyVPRM_examples repository, Glauch et al. (2025)).

A4.2 CH_4 Flux Models

Compute CH_4 emissions using the following: Wetlands: Kaplan (2002), Termites: Sanderson (1996) and Soil uptake: Ridgwell et al. (1999). This models require ERA5 soil temperature data, processed using scripts such as prep_wetland_kaplan.py and prep_T_ann.py.

A5 Anthropogenic Emissions

EDGAR GHG datasets are downloaded and converted using the download_edgar_ghg.sh and EDGARtoAE.py scripts, respectively.

A5.1 WetCHARTs Emissions

Obtain monthly CH_4 wetland emissions data from the WetCHARTs dataset and store them in the wetchart/ directory. This database includes biogenic emissions; however, to avoid substantial modifications to the WRF-GHG model structure, these emissions are stored within the "E_CH4TST" variable in "*wrfchemi*" file. Since individual tracers do not interact during model

https://doi.org/10.5194/egusphere-2026-979
Preprint. Discussion started: 10 April 2026

execution, this approach does not affect the model dynamics. This strategy was adopted to allow the incorporation of multiple externally derived biogenic methane fluxes while maintaining compatibility with the existing WRF-GHG framework.

A6 Biomass Burning (Fire) Emissions

GFAS fire data are downloaded using download_gfas_fire.py and processed with prep_gfas.py. CDS API access is required.

A7 Main Preprocessing Execution

The core script WRF_GHG_PrepPy.py is executed to generate the final WRF input files: wrfchemi_d0*, wrffire_d0*, and vprm_input_d0*.

A8 Background Concentration Fields

CAMS data for CO_2 and CH_4 are downloaded and interpolated to WRF domains using download_CAMS_with_cmmd.py, followed by calculate_CAMS_interpolation_indices.py, prep_initial_cond.py, and prep_boundary_cond.py. This sequence enables integration of all GHG-related emissions into WRF-GHG for accurate regional atmospheric simulations.

Appendix B: Standard metrics

- **Mean Bias (MB)**: The average difference between the observed and simulated concentrations. It provides an indication of the model's tendency to over- or underestimate the concentrations.

$$\mathrm{MB} = \frac{1}{N}\sum_{i=1}^{N}\left(C^i_{\mathrm{sim}} - C^i_{\mathrm{obs}}\right) \tag{B1}$$

  where C^i_{sim} and C^i_{obs} are the simulated and observed values at the i-th time step, respectively.

- **Pearson's correlation coefficient (r)**: This metric quantifies the strength and direction of the linear relationship between observed and simulated concentrations. A value close to +1 indicates a strong positive correlation.

$$r = \frac{\sum_{i=1}^{N}\left(C^i_{\mathrm{sim}} - \bar{C_{\mathrm{sim}}}\right)\left(C^i_{\mathrm{obs}} - \bar{C_{\mathrm{obs}}}\right)}{\sqrt{\sum_{i=1}^{N}\left(C^i_{\mathrm{sim}} - \bar{C_{\mathrm{sim}}}\right)^2 \sum_{i=1}^{N}\left(C^i_{\mathrm{obs}} - \bar{C_{\mathrm{obs}}}\right)^2}} \tag{B2}$$

  where $\bar{C_{\mathrm{sim}}}$ and $\bar{C_{\mathrm{obs}}}$ are the mean simulated and observed concentrations, respectively.

- **Root Mean Squared Error (RMSE)**: A measure of the differences between observed and simulated concentrations, with greater weight given to larger errors. This metric gives an indication of the magnitude of the error in the model simulation.

https://doi.org/10.5194/egusphere-2026-979
Preprint. Discussion started: 10 April 2026

$$\mathrm{RMSE} = \sqrt{\frac{1}{N}\sum_{i=1}^{N}\left(C^{i}_{\mathrm{sim}} - C^{i}_{\mathrm{obs}}\right)^{2}} \tag{B3}$$

All metrics were computed for the hourly model output against observed data.

Financial support. This research has been supported by the São Paulo Research Foundation (FAPESP, grant 2024/01369-2), linked to project 2022/07974-0.

Code and data availability. The WRF-Chem model code is publicly available through NCAR's repository (https://doi.org/10.5065/D6MK6B4K, NCAR, 2020). All external datasets required for running the WRF-GHG model are integrated into the GitHub repository, WRF-GHG-Prepy (https://github.com/rnoeliab/WRF-GHG-Prepy), which includes detailed documentation on each dataset and the associated configuration files for an easier setup. Meteorological and greenhouse gas (GHG) data from the ATTO site are accessible at https://www.attodata.org/. Additional data used in this study are available upon request from the corresponding author.

Author contributions. NRB wrote the initial manuscript and ran the WRF-GHG model to study the dynamics of greenhouse gases. NRB, in collaboration with SB, LVR, and LATM, developed the methodology. TG and SB contributed the pyVPRM package to estimate VPRM inputs from the WRF model. DH, MG, SB, and FAFDO collaborated on the creation of the WRF-GHG-Prepy GitHub repository. FSDS and ACPJ ran the JULES model for comparison with the VPRM module outputs. HvA, CQDJ, LO, and HF provided the observational data from the ATTO tower. AVV, SB, LVR, and LATM assisted in interpreting the results. All co-authors contributed to the review of the manuscript.

Competing interests. The authors declare that they have no conflict of interest.

Acknowledgements. We acknowledge the Physics Institute of the University of São Paulo for providing an academic environment. Our sincere thanks go to the Max Planck Institute for Biogeochemistry in Jena for providing access to the Levante supercomputer. We also thank the Instituto Nacional de Pesquisas da Amazônia (INPA) and the ATTO tower collaborators for providing the observational data. Finally, we are grateful for the financial support from the São Paulo Research Foundation (FAPESP, grant 2024/01369-2).

https://doi.org/10.5194/egusphere-2026-979
Preprint. Discussion started: 10 April 2026

References

Adams, D.K., Souza, Ê.P., & Costa, A. A. : Moist convection in Amazonia: implications for numerical modelling, Rev. Bras. Meteorol., 24, 168–178, 2009.

Ahmadov, R., Gerbig, C., Kretschmer, R., Koerner, S., Neininger, B., Dolman, A., & Sarrat, C.: Mesoscale covariance of transport and CO2 fluxes: Evidence from observations and simulations using the WRF-VPRM coupled atmosphere-biosphere model, J. Geophys. Res., https://doi.org/10.1029/2007JD008552, 2007.

Basso, L.S., Marani, L., Gatti, L.V., et al.: Amazon methane budget derived from multi-year airborne observations highlights regional variations in emissions, Commun. Earth Environ., 2, 246, https://doi.org/10.1038/s43247-021-00314-4, 2021.

Beck, V., Koch, T., Kretschmer, R., Marshall, J., Ahmadov, R., Gerbig, C., Pillai, D., & Heimann, M.: The WRF Greenhouse Gas Model (WRF-GHG), Tech. Rep. No. 25, Max Planck Institute for Biogeochemistry, Jena, Germany, 2011.

Beck, V., Chen, H., Gerbig, C., Bergamaschi, P., Bruhwiler, L., Houweling, S., Röckmann, T., Kolle, O., Steinbach, J., Koch, T., Sapart, C.J., van der Veen, C., Frankenberg, C., Andreae, M.O., Artaxo, P., Longo, K.M., & Wofsy, S.C.: Methane airborne measurements and comparison to global models during BARCA, J. Geophys. Res.-Atmos., 117, D15, https://doi.org/10.1029/2011JD017345, 2012.

Beck, V., Gerbig, C., Koch, T., Bela, M.M., Longo, K.M., Freitas, S.R., Kaplan, J.O., Prigent, C., Bergamaschi, P., & Heimann, M.: WRF-Chem simulations in the Amazon region during wet and dry season transitions: evaluation of methane models and wetland inundation maps, Atmos. Chem. Phys., 13, 7961–7982, https://doi.org/10.5194/acp-13-7961-2013, 2013.

Bergamaschi, P., Frankenberg, C., Meirink, J.F., Krol, M., Dentener, F., Wagner, T., Goede, A., & Schäfer, K.: Satellite cartography of atmospheric methane from SCIAMACHY on board ENVISAT: 2. Evaluation based on inverse model simulations, J. Geophys. Res.-Atmos., 112(D2), 2007.

Best, M.J., Pryor, M., Clark, D.B., Rooney, G.G., Essery, R.L.H., Menard, C.B., Edwards, J.M., Hendry, M.A., Porson, A., Gedney, N., Mercado, L.M., Sitch, S., Blyth, E., Boucher, O., Cox, P.M., Grimmond, C.S.B., & Harding, R.J.: The Joint UK Land Environment Simulator (JULES), model description – Part 1: Energy and water fluxes, Geosci. Model Dev., 4, 677–699, https://doi.org/10.5194/gmd-4-677-2011, 2011.

Bisht, J.S., Patra, P.K., Takigawa, M., Kanaya, Y., Yamaguchi, M., Machida, T., & Tanimoto, H.: CO2 high-resolution simulation using WRF-GHG over the Kanto region in Japan, Authorea Preprints, 2023.

Bisht, J.S., Patra, P.K., Takigawa, M., Kanaya, Y., Yamaguchi, M., Machida, T., & Tanimoto, H.: High-Resolution Simulation of CO2 Using WRF-GHG Over the Kanto Region in Japan, J. Geophys. Res.-Atmos., 130, 2025.

Bloom, A.A., K.W. Bowman, M. Lee, A.J. Turner, R. Schroeder, J.R. Worden, R.J. Weidner, K.C. McDonald, and D.J. Jacob. 2021. CMS: Global 0.5-deg Wetland Methane Emissions and Uncertainty (WetCHARTs v1.3.1). ORNL DAAC, Oak Ridge, Tennessee, USA. https://doi.org/10.3334/ORNLDAAC/1915. https://daac.ornl.gov/CMS/guides/MonthlyWetland_CH4_WetCHARTs.html (accessed December 8, 2025).

Botía, S., Gerbig, C., Marshall, J., Lavric, J. V., Walter, D., Pöhlker, C., Holanda, B., Fisch, G., de Araújo, A. C., Sá, M. O., Teixeira, P. R., Resende, A. F., Dias-Junior, C. Q., van Asperen, H., Oliveira, P. S., Stefanello, M., and Acevedo, O. C.: Understanding nighttime methane signals at the Amazon Tall Tower Observatory (ATTO), Atmos. Chem. Phys., 20, 6583–6606, https://doi.org/10.5194/acp-20-6583-2020, 2020.

Botía, S., Munassar, S., Koch, T., Custodio, D., Basso, L.S., Komiya, S., Lavric, J.V., Walter, D., Gloor, M., Martins, G., Naus, S., Koren, G., Luijkx, I.T., Hantson, S., Miller, J.B., Peters, W., Rödenbeck, C., & Gerbig, C.: Combined CO2 measurement record indicates Amazon

https://doi.org/10.5194/egusphere-2026-979
Preprint. Discussion started: 10 April 2026

forest carbon uptake is offset by savanna carbon release, Atmos. Chem. Phys., 25, 6219–6255, https://doi.org/10.5194/acp-25-6219-2025, 2025.

Botia, S., Dias-Junior, C. Q., Komiya, S., van der Woude, A., Terristi, M., de Kok, R., Koren, G., van Asperen, H., Jones, S. P., D'Oliveira, F. A. F., Weber, U., Marques-Filho, E., Toro, I. M. C., Araújo, A., Lavric, J., Walter, D., Li, X., Wigneron, J.-P., Stocker, B., de Souza, J. G., O'Sullivan, M., Sitch, S., Ciais, P., Chevallier, F., Li, W., Luijkx, I. T., Peters, W., Quesada, C. A., Zaehle, S., Trumbore, S. E., Bastos, A.: Reduced vegetation uptake during the extreme 2023 drought turns the Amazon into a weak carbon source. ESS Open Archive. doi: 10.22541/essoar.173757133.37080321/v1, 2025.

CAMS, 2020: CAMS global inversion-optimised greenhouse gas fluxes and concentrations. Copernicus Atmosphere Monitoring Service (CAMS) Atmosphere Data Store, DOI: 10.24381/ed2851d2 (Accessed on 25-07-2024).

CAMS, 2023a: CAMS CO_2 inversion system, Copernicus Atmosphere Monitoring Service, retrieved from https://confluence.ecmwf.int/display/CKB/Description+of+the+CO2+inversion+production+chain#DescriptionoftheCO2inversionproductionchain-Inversionmethod, 2023a.

CAMS, 2023b: CAMS CH_4 inversion system, Copernicus Atmosphere Monitoring Service, retrieved from https://confluence.ecmwf.int/display/CKB/Description+of+the+CH4+inversion+production+chain, 2023b.

Cecchini, M.A., and Coauthors: The ATTO-Campina site: A new observatory for tropical convection and gas-aerosol-cloud-precipitation interactions in the Amazon, Bull. Amer. Meteor. Soc., BAMS-D-24-0092.1, https://doi.org/10.1175/BAMS-D-24-0092.1, 2025.

Clark, D.B., Mercado, L.M., Sitch, S., Jones, C.D., Gedney, N., Best, M.J., Pryor, M., Rooney, G.G., Essery, R.L.H., Blyth, E., Boucher, O., Harding, R.J., Huntingford, C., & Cox, P.M.: The Joint UK Land Environment Simulator (JULES), model description – Part 2: Carbon fluxes and vegetation dynamics, Geosci. Model Dev., 4, 701–722, https://doi.org/10.5194/gmd-4-701-2011, 2011.

de Araújo, A.C., Kruijt, B., Nobre, A.D., Dolman, A.J., Waterloo, M.J., Moors, E.J., & de Souza, J.S.: Nocturnal accumulation of CO2 underneath a tropical forest canopy along a topographical gradient, Ecol. Appl., 18, 1406–1419, https://doi.org/10.1890/06-0982.1, 2008.

do Carmo, J.B., Keller, M., Dias, J.D., Camargo, P.B., & Crill, P.: A source of methane from upland forests in the Brazilian Amazon, Geophys. Res. Lett., 33, L04809, https://doi.org/10.1029/2005GL025436, 2006.

Curtius, J., Heinritzi, M., Beck, L.J., et al.: Isoprene nitrates drive new particle formation in Amazon's upper troposphere, Nature, 636,pe 124–130, https://doi.org/10.1038/s41586-024-08192-4, 2024.

Colas, F., Chanudet, V., Daufresne, M., Buchet, L., Vigouroux, R., Bonnet, A., et al.: Spatial and temporal variability of diffusive CO2 and CH4 fluxes from the Amazonian reservoir Petit-Saut (French Guiana) reveals the importance of allochthonous inputs for long-term C emissions, Global Biogeochem. Cycles, 34, e2020GB006602, https://doi.org/10.1029/2020GB006602, 2020.

Ferrario, F.M., Crippa, M., Guizzardi, D., Muntean, M., Schaaf, E., Lo Vullo, E., ... and Vignati, E.: EDGAR v6.0 Greenhouse Gas Emissions, European Commission, Joint Research Centre (JRC) [data set], http://data.europa.eu/89h/97a67d67-c62e-4826-b873-9d972c4f670b, last access: November 2024, 2021.

Gatti, L.V., Basso, L.S., Miller, J.B., et al.: Amazonia as a carbon source linked to deforestation and climate change, Nature, 595, 388–393, https://doi.org/10.1038/s41586-021-03629-6, 2021.

Gerbig, C., Körner, S., and Lin, J. C.: Vertical mixing in atmospheric tracer transport models: error characterization and propagation, Atmos. Chem. Phys., 8, 591–602, https://doi.org/10.5194/acp-8-591-2008, 2008.

Gerken, T., Feng, S., Keller, K., Lauvaux, T., DiGangi, J. P., Choi, Y., et al.: Examining CO2 model observation residuals using ACT-America data. Journal of Geophysical Research: Atmospheres, 126, e2020JD034481. https://doi.org/10.1029/2020JD034481, 2021.

https://doi.org/10.5194/egusphere-2026-979
Preprint. Discussion started: 10 April 2026

Glauch, T., Marshall, J., Gerbig, C., Botía, S., Gałkowski, M., Vardag, S.N., & Butz, A.: pyVPRM: A next-generation Vegetation Photosynthesis and Respiration Model for the post-MODIS era, Geosci. Model Dev., 18(14), 4713–4742, 2025.

Harper, A.B., Cox, P.M., Friedlingstein, P., Wiltshire, A.J., Jones, C.D., Sitch, S., Mercado, L.M., Groenendijk, M., Robertson, E., Kattge, J., Bönisch, G., Atkin, O.K., Bahn, M., Cornelissen, J., Niinemets, Ü., Onipchenko, V., Peñuelas, J., Poorter, L., Reich, P.B., Soudzilovskaia, N.A., and Bodegom, P.V.: Improved representation of plant functional types and physiology in the Joint UK Land Environment Simulator (JULES v4.2) using plant trait information, Geosci. Model Dev., 9, 2415–2440, https://doi.org/10.5194/gmd-9-2415-2016, 2016.

Hernández, K.S., Gómez-Ríos, S., Henao, J.J., Robledo V., Ramírez-Cardona, A., Rendón, A.M.: Rainfall Sensitivity to Microphysics and Planetary Boundary Layer Parameterizations in Convection-Permitting Simulations over Northwestern South America, J. Meteorol. Res., 38, 805–825, https://doi.org/10.1007/s13351-024-3156-4, 2024.

Hersbach, H., Bell, B., Berrisford, P., et al.: The ERA5 global reanalysis, Q. J. R. Meteorol. Soc., 146, 1999–2049, https://doi.org/10.1002/qj.3803, 2020.

Ho, D., Gałkowski, M., Reum, F., Botía, S., Marshall, J., Totsche, K. U., and Gerbig, C.: Recommended coupling to global meteorological fields for long-term tracer simulations with WRF-GHG, Geosci. Model Dev., 17, 7401–7422, https://doi.org/10.5194/gmd-17-7401-2024, 2024.

Huffman, G.J., Bolvin, D.T., Nelkin, E.J., et al.: Integrated Multi-satellite Retrievals for GPM (IMERG), Version 06, NASA Goddard Earth Sciences Data and Information Services Center (GES DISC), 2019.

Masson-Delmotte, V., Zhai, P., Pirani, A., Connors, S.L., Péan, C., Berger, S., Caud, N., Chen, Y., Goldfarb, L., Gomis, M.I., et al.: IPCC Climate Change 2021: The Physical Science Basis. Contribution of Working Group I to the Sixth Assessment Report of the Intergovernmental Panel on Climate Change, Eds. Cambridge University Press: Cambridge, UK, 2021.

Janssens-Maenhout, G., Crippa, M., Guizzardi, D., Muntean, M., Schaaf, E., Dentener, F., Bergamaschi, P., Pagliari, V., Olivier, J., Peters, J., van Aardenne, J., Monni, S., Doering, U., Petrescu, R., Solazzo, E., & Oreggioni, G.: EDGAR v4.3.2 Global Atlas of the Three Major Greenhouse Gas Emissions for the Period 1970–2012, Earth Syst. Sci. Data Discuss., https://doi.org/10.5194/essd-2018-164, 2019.

Kaiser, J.W., Heil, A., Andreae, M.O., Benedetti, A., Chubarova, N., Jones, L., Morcrette, J.-J., Razinger, M., Schultz, M.G., Suttie, M., and van der Werf, G.R.: Biomass burning emissions estimated with a global fire assimilation system based on observed fire radiative power, Biogeosciences, 9, 527–554, https://doi.org/10.5194/bg-9-527-2012, 2012.

Kaplan, J.O.: Wetlands at the Last Glacial Maximum: Distribution and methane emissions, Geophys. Res. Lett., 29, 1079, https://doi.org/10.1029/2001GL013366, 2002.

Mahadevan, P., Wofsy, S.C., Matross, D.M., Xiao, X., Dunn, A.L., Lin, J.C., ... and Gottlieb, E.W.: A satellite-based biosphere parameterization for net ecosystem CO2 exchange: Vegetation Photosynthesis and Respiration Model (VPRM), Global Biogeochem. Cycles, 22(2), https://doi.org/10.1029/2006GB002735, 2008.

Mai, B., Deng, X., Diao, Y., Yin, S., Liu, X.: Optimization of VPRM Parameters for the Simulation of Atmospheric CO2 Flux in the Pearl River Delta Region of China, available at SSRN: https://ssrn.com/abstract=4326647, 2023.

Masarie, K. A., Petron, G., Andrews, A., Bruhwiler, L., Conway, T. J., Jacobson, A. R., Miller, J. B., Tans, P. P., Worthy, D. E., & Peters, W.: Impact of CO2 measurement bias on CarbonTracker surface flux estimates. Journal of Geophysical Research: Atmospheres, 116(D17), Article D17305. https://doi.org/10.1029/2011JD016270, 2011.

Mendonça, A. C., Dias-Júnior, C. Q., Acevedo, O. C., Marra, D. M., Cely-Toro, I. M., Fisch, G., Brondani, D. V., Manzi, A. O., Portela, B. T., Quesada, C. A., Mortarini, L. (2025). Estimation of the nocturnal boundary layer height over the Central Amazon forest using turbulence measurements. Agricultural and Forest Meteorology, 367: 110469. doi: 10.1016/j.agrformet.2025.110469.

https://doi.org/10.5194/egusphere-2026-979
Preprint. Discussion started: 10 April 2026

Miles, N. L., Davis, K. J., Richardson, S. J., Lauvaux, T., Martins, D. K., Deng, A. J., Balashov, N., Gurney, K. R., Liang, J., Roest, G., Wang, J. A., & Turnbull, J. C.: The influence of near-field fluxes on seasonal carbon dioxide enhancements: results from the Indianapolis Flux Experiment (INFLUX). Carbon balance and management, 16(1), 4. https://doi.org/10.1186/s13021-020-00166-z, 2021.

Miller, J.B., Gatti, L.V., d'Amelio, M.T.S., Crotwell, A.M., Dlugokencky, E.J., Bakwin, P., Artaxo, P., and Tans, P.P.: Airborne measurements indicate large methane emissions from the eastern Amazon basin, Geophys. Res. Lett., 34, 10, https://doi.org/10.1029/2006GL029213, 2007.

Molina, L., Broquet, G., Imbach, P., Chevallier, F., Poulter, B., Bonal, D., Burban, B., Ramonet, M., Gatti, L.V., Wofsy, S.C., Munger, J.W., Dlugokencky, E., and Ciais, P.: On the ability of a global atmospheric inversion to constrain variations of CO2 fluxes over Amazonia, Atmos. Chem. Phys., 15, 8423–8438, https://doi.org/10.5194/acp-15-8423-2015, 2015.

Nussbaumer, C.M., Kohl, M., Pozzer, A., Tadic, I., Rohloff, R., Marno, D., et al.: Ozone formation sensitivity to precursors and lightning in the tropical troposphere based on airborne observations. Journal of Geophysical Research: Atmospheres, 129, e2024JD041168. https://doi.org/10.1029/2024JD041168, 2024.

de Oliveira E. A., Feldpausch TR, Marimon BS, Morandi PS, Phillips OL, Bird M, Murakami AA, Arroyo L, Quesada CA and Marimon-Junior BH.: Soil pyrogenic carbon in southern Amazonia: Interaction between soil, climate, and above-ground biomass. Front. For. Glob. Change 5:880963. doi: 10.3389/ffgc.2022.880963, 2022.

Ort, L., Röder, L. L., Parchatka, U., Königstedt, R., Crowley, D., Kunz, F., Wittkowski, R., Lelieveld, J., and Fischer, H.: In-flight characterization of a compact airborne quantum cascade laser absorption spectrometer, Atmos. Meas. Tech., 17, 3553–3565, https://doi.org/10.5194/amt-17-3553-2024, 2024.

Park, C., Gerbig, C., Newman, S., Ahmadov, R., Feng, S., Gurney, K.R., Carmichael, G.R., Park, S., Lee, H., Goulden, M., Stutz, J., Peischl, J., & Ryerson, T.: CO2 Transport, Variability, and Budget over the Southern California Air Basin Using the High-Resolution WRF-VPRM Model during the CalNex 2010 Campaign, J. Appl. Meteorol. Climatol., 57, 1–19, https://doi.org/10.1175/JAMC-D-17-0358.1, 2018.

Prudente Junior, A.C., Machado, L.A.T., Silva, F.S., Ambrizzi, T., Artaxo, P., Botia, S., Cordeiro, L.P., Dias Junior, C.Q., Freitas, E., Moreira, D.S., Pöhlker, C., Toro, I.M.C., Xu, X., and Rizzo, L.V.: Spatializing Net Ecosystem Exchange in the Brazilian Amazon biome using the JULES model and vegetation properties, EGUsphere [preprint], https://doi.org/10.5194/egusphere-2025-2869, 2025.

Querino, C.A., Smeets, C., Vigano, I., Holzinger, R., Moura, V.S., Gatti, L.V., Martinewski, A., Manzi, A.O., Araújo, A.C., & Röckmann, T.: Methane flux, vertical gradient and mixing ratio measurements in a tropical forest, Atmos. Chem. Phys., 11, 7943–7953, https://doi.org/10.5194/acp-11-7943-2011, 2011.

Ridgwell, A.J., Marshall, S.J., & Gregson, K.: Consumption of atmospheric methane by soils: A process-based model, Global Biogeochem. Cycles, 13(1), 59–70, https://doi.org/10.1029/1998GB900004, 1999.

Rödenbeck, C., Gerbig, C., Trusilova, K., and Heimann, M.: A two-step scheme for high-resolution regional atmospheric trace gas inversions based on independent models, Atmos. Chem. Phys., 9, 5331–5342, https://doi.org/10.5194/acp-9-5331-2009, 2009.

Sakaguchi, K., Leung, L.R., Burleyson, C.D., Xiao, H., & Wan, H.: Role of Troposphere-Convection-Land Coupling in the Southwestern Amazon Precipitation Bias of the Community Earth System Model Version 1 (CESM1), J. Geophys. Res. Atmos., 123, 8374–8399, https://api.semanticscholar.org/CorpusID:135374493, 2018.

Sanderson, M.G.: Biomass of termites and their emissions of methane and carbon dioxide: A global database, Global Biogeochem. Cycles, 10(4), 543–557, https://doi.org/10.1029/96GB01893, 1996.

Seo, M.G., Kim, H.M., Kim, D.H.: Effect of atmospheric conditions and VPRM parameters on high-resolution regional CO2 simulations over East Asia, Theor. Appl. Climatol., 155, 859–877, https://doi.org/10.1007/s00704-023-04663-2, 2024.

https://doi.org/10.5194/egusphere-2026-979
Preprint. Discussion started: 10 April 2026

Sousa, J., Candido, L., Silva, J.T., Andreoli, R.V., Kayano, M.T., Manzi, A.O., Souza, R., Vieira, S.: Avaliação da habilidade do modelo WRF em representar a precipitação na Amazônia usando diferentes escalas, Rev. Bras. Meteorol., 34, 255–265, https://doi.org/10.1590/0102-77863340029, 2019.

Souza, C. M., Jr., Z. Shimbo, J., Rosa, M. R., Parente, L. L., A. Alencar, A., Rudorff, B. F. T., Hasenack, H., Matsumoto, M., G. Ferreira, L., Souza-Filho, P. W. M., de Oliveira, S. W., Rocha, W. F., Fonseca, A. V., Marques, C. B., Diniz, C. G., Costa, D., Monteiro, D., Rosa, E. R., Vélez-Martin, E., ... Azevedo, T.: Reconstructing Three Decades of Land Use and Land Cover Changes in Brazilian Biomes with Landsat Archive and Earth Engine. Remote Sensing, 12(17), 2735. https://doi.org/10.3390/rs12172735, 2020.

Souza, C. M. A.; Dias-Júnior, C. Q.; D'Oliveira, F. A. F.; Martins, H. S.; Carneiro, R. G.; Portela, B. T. T.; Fisch, G.: Long-term measurements of the atmospheric boundary layer height in Central Amazonia using remote sensing instruments. Remote Sensing 15 (13). doi: 10.3390/rs15133261, 2023.

Tóta, J., Fitzjarrald, D.R., da Silva Dias, M.A.: Amazon rainforest exchange of carbon and subcanopy air flow: Manaus LBA site–a complex terrain condition, Scientific World J., 2012, https://doi.org/10.1100/2012/165067, 2012.

van Asperen, H., Jones, S., Lavric, J., Walter, D., Sierra, Carlos., Horna, V., Komiya, S., Botia, S., Warneke, T., Griffith, D., Heimann, M., Andreae, M., & Trumbore, S.: Long term continuous high-precision greenhouse gas observation at the ATTO fieldsite: an overview. , BOOK OF ABSTRACTS - 11TH INTERNATIONAL CARBON DIOXIDE CONFERENCE., https://proceedings.science/icdc-2024/papers/long-term-continuous-high-precision-greenhouse-gas-observation-at-the-atto-field?lang=en, 2024.

Wilson, C., M. Gloor, L. V. Gatti, J. B. Miller, S. A. Monks, J. McNorton, A. A. Bloom, L. S. Basso, and M. P. Chipperfield,: Contribution of regional sources to atmospheric methane over the Amazon Basin in 2010 and 2011, Global Biogeochem. Cycles, 30, 400–420, doi:10.1002/2015GB005300, 2016.

Wu, G., Hu, Z., Keenan, T.F., Li, S., Zhao, W., Cao, R.C., Li, Y., Guo, Q., & Sun, X.: Incorporating spatial variations in parameters for improvements of an evapotranspiration model, J. Geophys. Res. Biogeosciences, 125, https://doi.org/10.1029/2019JG005504, 2020.

Zhao, M., & Running, S. W.: Drought-induced reduction in global terrestrial net primary production from 2000 through 2009. Science (New York, N.Y.), 329(5994), 940–943. https://doi.org/10.1126/science.1192666, 2010.